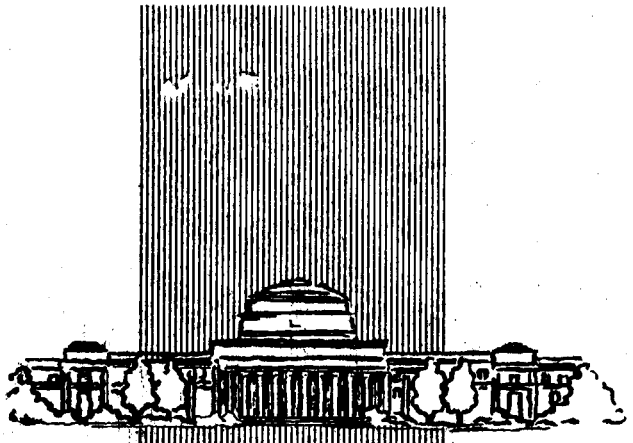

# MASSACHUSETTS INSTITUTE OF TECHNOLOGY

RE-52

## ERROR ANALYSIS OF STRAPDOWN AND LOCAL LEVEL INERTIAL SYSTEMS WHICH COMPUTE IN GEOGRAPHIC COORDINATES

by

KENNETH R. BRITTING



NOVEMBER 1969

**MEASUREMENT SYSTEMS LABORATORY**

MASSACHUSETTS INSTITUTE OF TECHNOLOGY
CAMBRIDGE 39, MASSACHUSETTS

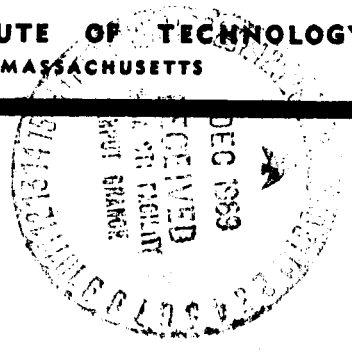

RE-52

# ERROR ANALYSIS OF STRAPDOWN AND LOCAL LEVEL INERTIAL SYSTEMS WHICH COMPUTE IN GEOGRAPHIC COORDINATES

by

Kenneth R. Britting

November, 1969

Approved: W. Markey

Director
Measurement Systems Laboratory

## Abstract

This report is a tutorial exposition of two broad classes of strapdown and local level inertial navigation systems, which perform their navigational computations in the local geographic coordinate frame. The strapdown chapter includes discussions of the direction cosine update procedure, alignment techniques and instrument redundancy. An analysis of error sources peculiar to the strapdown mechanization is followed by a perturbation type error analysis which shows that the basic error equations are identical to those which describe the behavior of the local level platform system. The error analysis of the local level system is followed by a rather complete set of analytic and computer solutions for both the stationary and moving navigation cases. The effect of the Foucault mode on the validity of the analytic solutions is discussed. The results of the error analysis are applicable to both navigation system mechanizations.

## Acknowledgements

This report was prepared under DSR Project No. 70343 sponsored by the National Aeronautics and Space Administration Electronic Research Center, Cambridge, Massachusetts, through NASA Grant No. NGR 22-009-229.

The publication of this report does not constitute approval by the National Aeronautics and Space Administration or by the MIT Measurement Systems Laboratory of the findings or the conclusions contained therein. It is published only for the exchange and stimulation of ideas.

Table of Contents

# 1 STRAPDOWN INERTIAL NAVIGATION SYSTEM

## 1.1 Introduction

Strapdown systems are characterized by their lack of gimbal support structure. The system is mechanized by mounting three gyros and three accelerometers directly to the vehicle for which the navigation function is to be provided. An onboard digital computer keeps track of the vehicle's attitude with respect to some reference frame based on information from the gyros. The computer is thus able to provide the coordinate transformation necessary to coordinatize the accelerometer outputs in a reference frame. Navigation computations proceed in exactly the same fashion as for the platform systems discussed previously.

Conceptually, the system is no more complicated than those which have been studied previously. Figure 1.1 shows a functional block diagram for a typical strapdown system. Note that the navigational computations can take place in either geographic coordinates or inertial coordinates, depending on the application. For airborne applications, altimeter error sensitivity considerations would make it seem reasonable to compute in geographic coordinates. Thus a strapdown inertial navigation system which computes in geographic coordinates will be considered herein.

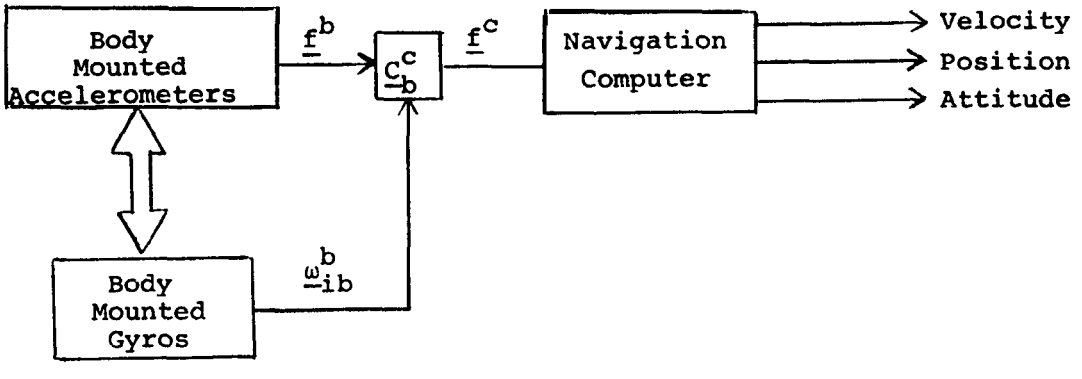


Figure 1.1 ∿ Strapdown System Functional Diagram

Many arguments are heard, both pro and con, concerning the viability of strapdown systems. Weight and size comparisons between strapdown and gimbal systems involve a trade-off between a more extensive computer for the strapdown system versus the gimbal structure for the conventional system. With the advent of microcircuits, the advantage of the strapdown system would appear to be increasing. The strapdown system also would appear to have a definite advantage over the gimbal system in terms of power consumption, packaging flexibility, ease of maintenance, and perhaps cost. It should be pointed out, however, that those considerations should be weighed according to accuracy. Strapdown systems are not yet capable of competing with conventional systems in applications where accuracy is the primary criterion of excellence. From a reliability standpoint, it would seem that the binary devices in a strapdown system would be less susceptible to such factors as line voltage variations, power supply transients, etc. Since the strapdown sensors remain fixed with respect to the vehicle, one would expect that the environmental control problem would be eased considerably.

The major disadvantage of the strapdown system is summarized with one word--inaccuracy. The instruments are subjected to a relatively harsh dynamic environment since the gimbal structure no longer isolates the sensors from the angular motion and vibrations of the vehicle. Because of this different environment, the instruments must be designed with a larger dynamic range, which usually results in a compromise in accuracy. It should be pointed out, however, that most testing to date has been done with instruments that were designed for use in gimballed systems. Current design research toward the development of sensors which have improved performance in the strapdown environment may alter the current "accuracy gap" which exists between gimballed and strapdown systems.

To illustrate how the instruments will be affected by the strapdown environment, take the case of a single degree of freedom floated integrating gyro. The output of such an instrument is

given by Reference 5 as:

$$(\tau_g\, p + 1)A_g = \frac{H}{pC_g}\,(\omega_{IA} - \omega_c - A_g\,\omega_{SRA} + (u)\omega) - \tau_g\,\omega_{OA}$$

where

$\tau_g$ ∿ Time constant of gyro

$p$ ∿ Differential operator ∿ $\frac{d}{dt}$

$A_g$ ∿ Gyro output angle

$H$ ∿ Spin angular momentum

$C_g$ ∿ Damping coefficient

$\omega_{IA}$ ∿ Input axis angular velocity

$\omega_c$ ∿ Command angular velocity

$\omega_{SRA}$ ∿ Spin reference axis angular velocity

$(u)\omega$ ∿ Uncertainty angular velocity

$\omega_{OA}$ ∿ Output axis angular velocity

The gyro equation can be rearranged in the signal flow diagram shown in figure 1.2

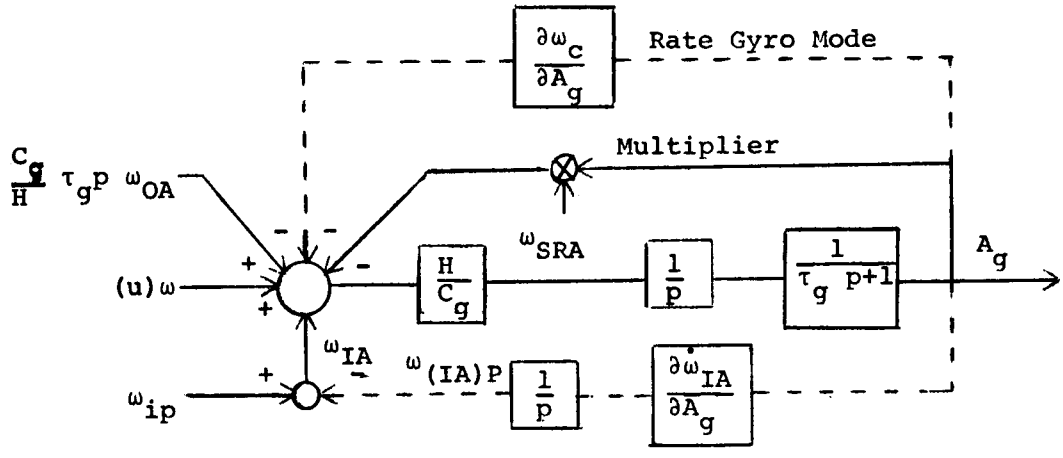


Figure 1.2 ∿ Signal Flow Diagram for Integrating Gyro

As indicated on the diagram, the gyro can be used in either of two modes, the space integrator mode or the rate gyro mode. If we instrument as a space integrator, the appropriate gimbal is torqued with a signal proportional to $A_g$, driving $\omega_{IA}$ to zero. It is evident that in steady state:

$$\omega_{IA} = - (u)\omega,$$

$A_g$ being driven to zero. Note that the accuracy in applying the torque to the gimbal has no effect on the final result. Moreover, if the gyro is visualized as being mounted on an uncommanded space integrator,

$$\omega_{OA} = \omega_{SRA} = \omega_{IA} \simeq 0$$

if gyro drift is neglected.

If, on the other hand, we instrument as a rate gyro applying a signal to the gyro torque generator proportional to $A_g$, we require that in steady state:

$$\omega_{IA} + (u)\omega = \frac{\partial \omega_c}{\partial A_g} A_g$$

We see then that the uncertainty in $\partial\omega_c/\partial A_g$, that is, our knowledge of the torquer sensitivity, is of crucial importance in determining $\omega_{IA}$. Furthermore, if the instrument is body mounted, one has the linear disturbance input equal to $\tau_b \dot{\omega}_{OA}$ and the nonlinear disturbance input due to $A_g \omega_{SRA}$. The linear disturbance is compensated, while the nonlinear disturbance is minimized by keeping $A_g$ small through servo design techniques.

A significant gyro problem that arises due to the strapdown environment is called input-spin rate rectification. This problem is a manifestation of the nonlinear disturbance phenomenon mentioned in the previous paragraph. One can see from figure (21) that, if $A_g$ and $\omega_{SRA}$ are oscillating simultaneously, a spurious input angular velocity will be sensed. This effect can be quite large, depending on the frequency of vibration.

In addition to the problems that arise due to the cross-coupling effects mentioned above, vibration-induced errors are likely to be quite troublesome for strapdown gyros. These errors mainly result from the anisoelastic properties of the gyro float. In general, torquing is applied to the gyroscopes to compensate for this inherent deterministic drift via the following equation (Ref. 6):

$$T_k = B_k + M_{k_S} f_{k_S} - M_{k_I} f_{K_I} + (K_{k_S} - K_{k_I}) f_{k_I} f_{k_S}, \quad k = x, y, z$$

where

$T_k$ ∿ commanded torque to $k^{th}$ gyro

$B_k$ ∿ bias torque coefficient for $k^{th}$ gyro

$M_{k_S}$ ∿ mass unbalance torque coefficient along spin axis for $k^{th}$ gyro

$M_{k_I}$ ∿ mass unbalance torque coefficient along input axis for $k^{th}$ gyro

$f_{k_I}$ ∿ specific force along input axis of $k^{th}$ gyro

$f_{k_S}$ ∿ specific force along spin axis of $k^{th}$ gyro

$K_{k_S}$ ∿ anisoelastic torque coefficient along spin axis of $k^{th}$ gyro

$K_{k_I}$ ∿ anisoelastic torque coefficient along input axis of $k^{th}$ gyro

In the above equation, the so-called "cross compliance" terms have been excluded. Depending on the application and the quality of the gyroscopes, these terms might have to be included. The terms in the $T_k$ expression must, in general, be calculated and introduced

as compensation terms. The problems inherent in computing and applying the compensation are discussed in Reference 7. Because of the difficulty in applying the compensation, vibratory effects are usually beyond the bandwidth of the compensating system.

Such effects as mentioned above must be considered in the design of any inertial system. For the strapdown system, environmental considerations are likely to consume a high percentage of the design time. The reader is referred to Ref. 8 for a more complete exposition of this subject.

## 1.2 Description of System

As mentioned previously, the inertial sensors of a strapdown system are mounted directly to the vehicle. The accelerometers and gyroscopes are typically mounted in a mutually orthogonal fashion, although in certain cases where reliability is of utmost importance extra instruments are added to form a nonorthogonal cluster of four instruments. Thus the fourth instrument is capable of taking the place of any instrument in the orthogonal set which fails. In addition, the output of the fourth instrument can be continuously used for averaging purposes.

In any case, the outputs of the accelerometers, suitably coordinatized and averaged, are equal to the nonfield specific force coordinatized in body axes:

$$\underline{f}^b = \underline{C}_i^b \, (\ddot{\underline{r}}^i - \underline{G}^i) \tag{1.1}$$

The computer must then transform the specific force into a suitable reference frame such that navigational information may be extracted. If rate gyro information is available, then the direction cosine matrix, $\underline{C}_b^i$, can be specified. The relationship between angular velocity and the direction cosine matrix is specified by:

$$\dot{\underline{C}}_b^i = \underline{C}_b^i \, \underline{\Omega}_{ib}^b \tag{1.2}$$

where

$$\underline{\Omega}_{ib}^b = \begin{bmatrix} 0 & -\omega_z & \omega_y \\ \omega_z & 0 & -\omega_x \\ -\omega_y & \omega_x & 0 \end{bmatrix} \tag{1.3}$$

$$\underline{\omega}_{ib}^b = \{\omega_x, \, \omega_y, \, \omega_z\} \tag{1.4}$$

Equation (122) is a first order matrix differential equation in $\underline{C}_b^i$. It can alternately be interpreted as a shorthand way of writing nine simultaneous differential equations in nine unknowns, as can be seen by writing equation 1.2 in component form:

$$\begin{bmatrix} \dot{C}_{11} & \dot{C}_{12} & \dot{C}_{13} \\ \dot{C}_{21} & \dot{C}_{22} & \dot{C}_{23} \\ \dot{C}_{31} & \dot{C}_{32} & \dot{C}_{33} \end{bmatrix} = \begin{bmatrix} C_{11} & C_{12} & C_{13} \\ C_{21} & C_{22} & C_{23} \\ C_{31} & C_{32} & C_{33} \end{bmatrix} \begin{bmatrix} 0 & -\omega_z & \omega_y \\ \omega_z & 0 & -\omega_x \\ -\omega_y & \omega_x & 0 \end{bmatrix}$$

$$= \begin{bmatrix} C_{12}\omega_z - C_{13}\omega_y & C_{13}\omega_x - C_{11}\omega_z & C_{11}\omega_y - C_{12}\omega_x \\ C_{22}\omega_z - C_{23}\omega_y & C_{23}\omega_x - C_{21}\omega_z & C_{21}\omega_y - C_{22}\omega_x \\ C_{32}\omega_z - C_{33}\omega_y & C_{33}\omega_x - C_{31}\omega_z & C_{31}\omega_y - C_{32}\omega_x \end{bmatrix}$$

It should be pointed out in passing that other schemes can be used to effect the coordinate transformation. Weiner (Ref. 9) has studied the available choices and concludes that, for single-degree-of-freedom, delta-modulated instruments, utilizing a D.D.A. computer, the direction cosine approach requires minimum computation. Because of our familiarity with the direction cosine method, we will use it in our considerations of the strapdown inertial navigation system.

The direction cosine transformation is found quite easily for systems which use electrostatic gyroscopes (Ref 10), since clever pickoff schemes allow the direction cosines (elements of the $C_b^i$ matrix) to be read off directly. The output of each E.S.G.

pickoff is the direction cosine between the spin axis and an appropriate fiducial on the instrument case. Although there are three of these pickoffs per E.S.G., in general, only two of the three pickoffs provide useful information at any given time. Thus, if two E.S.G.'s are used, only four direction cosines will be available for computation at any time. The remaining five are found through application of the orthogonality relationship for coordinate transformation matrices:

$$\underline{C}_b^i \; [\underline{C}_b^i]^T = \underline{I} \tag{1.5}$$

The solution of equation (1.2) for the direction cosines can be done in a variety of ways. If single-degree-of-freedom, delta-modulated instruments are used, the gyro output angle is sampled and passed into a zero order hold circuit. Pulse torquing is then applied to the gyro float to null the instrument. Weiner shows that for this mechanization each output pulse is proportional to the integral of the input angular velocity. Thus the output of the instrument represents an angular rotation about the input axis equal to $\Delta\theta$. This property can be exploited in the solution for the direction cosine matrix if one considers a Taylor series expansion of $\underline{C}_b^i$ in $\Delta t$:

$$\underline{C}(t + \Delta t) = \underline{C}(t) + \dot{\underline{C}}(t)\,\Delta t + \frac{1}{2}\ddot{\underline{C}}(t)\,\Delta t^2 + \frac{1}{3!}\dddot{\underline{C}}\,\Delta t^3 + \ldots. \tag{1.6}$$

where $\underline{C}_b^i = \underline{C}$ for notational simplicity.

But application of equation (123) yields:

$$\underline{C}(t + \Delta t) = \underline{C}(t)\left[\underline{I} + \underline{\Omega}\,\Delta t + \frac{1}{2}(\underline{\Omega}^2 + \dot{\underline{\Omega}})\Delta t^2 + \ldots..\right] \tag{1.7}$$

If the first two terms of the expansion are used,

$$\underline{C}(t + \Delta t) = \underline{C}(t) + \underline{C}(t)\;\underline{\Delta\theta} \tag{1.8}$$

where it was noted that:

$$\underline{\Omega}\;\Delta t = \underline{\Delta\theta}$$

and $\Delta\underline{\theta}$ is a skew symmetric matrix composed of the gyro outputs $\Delta\theta_k$, k = x, y, z. The result shown in equation (1.8) could, of course, have been shown by direct differentiation of equation (1.2)

If the computational algorithm of equation (1.8) is used, which corresponds to a rectangular integration scheme, then the algorithm error (truncation error) is approximately given by the third term of equation (1.7):

$$\underline{\delta C} = \frac{1}{2}\,\underline{C}(\underline{\Omega}^2 + \dot{\underline{\Omega}})\Delta t^2 \tag{1.9}$$

Thus the time step, $\Delta t$, must be chosen such that the errors resulting from the vehicle angular velocity, $\underline{\Omega}$, and the vehicle angular acceleration, $\dot{\underline{\Omega}}$, satisfy the error budget. In addition, the finite computer word length causes the occurrence of "round-off" error.

## 1.3 Alignment

The problem of alignment in a strapdown inertial navigation system is basically that of determining the initial transformation matrix which relates the instrumented body frame to the reference computational frame. Because the inertial instruments are mounted directly to the vehicle, ordinary gyrocompassing methods cannot be used. Moreover, if we address ourselves to commercial applications of inertial navigation which are likely to appear in the next decade, it is clear that a means of self-alignment will be essential.

Indeed, it would appear that initial alignment within the environment and time constraints imposed by commercial aircraft operation is one of the more critical problems that will face the designers of these systems. The problem is one of determining a suitably accurate initial transformation matrix in the short period of time necessary for commercial success of the aircraft in the face of deleterious motions of the aircraft caused by wind gusts, the loading of passengers and cargo, fuel ingestion, etc.

A two-stage alignment scheme appears promising in this regard (Ref. 11). The first or "coarse" alignment stage would use an analytic alignment scheme which utilizes the measurement of the gravity and earth rotation vectors to directly compute the transformation matrix relating the body frame to the geographic frame. The same reservations concerning base motion mentioned in this reference are, of course, applicable here; however, the analytic method is well suited to calculating an initial estimate of the transformation matrix. The second or "corrective" alignment stage refines the initial estimate of the transformation matrix by using estimates of the error angles between the known reference frame and the corresponding computed frame.

For both alignment schemes, the instrumented frame is taken to be stationary with respect to the Earth except for the disturbances mentioned previously. Unfortunately, no data is available at this time on aircraft motion due to wind gusts and other disturbances. We will model the base motion as simple additive

vectors:

$$\underline{f} = -\underline{g} + \underline{f}_d \tag{1.10}$$

$$\underline{\omega}_{ib} = \underline{\omega}_{ie} + \underline{\omega}_d \tag{1.11}$$

where

$\underline{f}_d$ ∿ disturbance specific force vector

$\underline{\omega}_d = \underline{\omega}_{eb}$ ∿ disturbance angular velocity

If the geographic frame is used as a reference frame, then the corrective alignment scheme can be mechanized as shown in figure 1.3

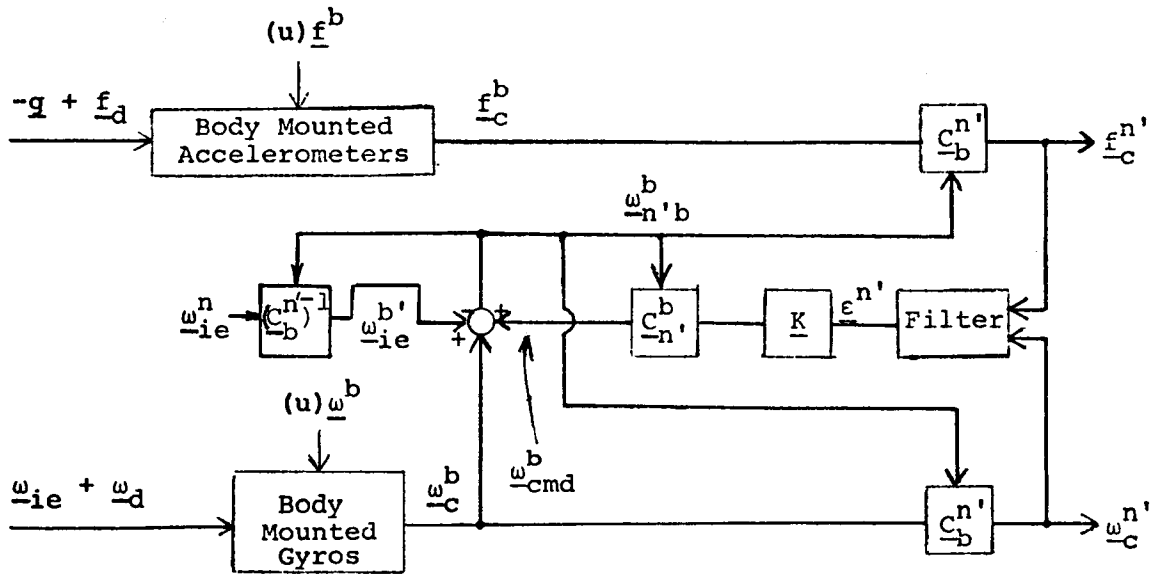


Figure 1.3 ∿ Self-Corrective Alignment Scheme

Because an initial estimate of the transformation matrix is available, we can model the misalignment between the actual and computed geographic frame as a small angle rotation. The updating method consists of detecting the error angles between these two frames via the processed accelerometer and gyro signals

and generating a signal to the transformation computer in order to drive these angles as close to zero as possible. At the same time, compensation is provided for the disturbance angular vibrations. This angular motion compensation provides "base motion isolation" similar to that provided in a gimballed platform system.

As shown in figure 1.3, the transformation matrix $\underline{C}_b^{n'}$ is updated using the relation:

$$\dot{\underline{C}}_b^{n'} = \underline{C}_b^{n'} \, \underline{\Omega}_{n'b}^{b} \tag{1.12}$$

where

- $n$ ∿ geographic axes
- $n'$ ∿ computed geographic axes
- $\underline{\Omega}_{n'b}^{b}$ ∿ skew symmetric matrix of the angular velocity $\underline{\omega}_{n'b}^{b}$ which is used to compute the transformation

The angular velocity signal used to update the transformation matrix would ideally be given by:

$$\underline{\omega}_{nb}^{b} = \underline{\omega}_{d}^{b} \tag{1.13}$$

where it was noted that:

$$\underline{\omega}_{ne} = \underline{0}$$

Note that $\underline{\omega}_{n'n}^{b}$ is ideally driven to zero by appropriate choice of $\underline{K}$. As shown in the figure, an estimate of $\underline{\omega}_d$ is obtained by subtracting $\underline{\omega}_{ie}^{b'}$, which is coordinatized in computed body coordinates, from the gyro's indication of angular velocity. But since $\underline{\omega}_{ie}^{b'}$ is not equal to $\underline{\omega}_{ie}^{b}$ and, in addition, $\underline{\omega}_c$ is corrupted by gyro drift $(u)\underline{\omega}^b$, the angular velocity signal used to update the transformation matrix is given by:

$$\underline{\omega}_{n'b}^{b} = \underline{\omega}_{cmd}^{b} + \underline{\omega}_{d}^{b} + (u)\underline{\omega}^{b} + \underline{\omega}_{ie}^{b} - (\underline{C}_b^{n'})^{-1} \, \underline{\omega}_{ie}^{n} \tag{1.14}$$

but

$$(\underline{C}_b^{n'})^{-1} \, \underline{\omega}_{ie}^{n} = (\underline{C}_n^{n'} \underline{C}_b^{n})^{-1} \, \underline{\omega}_{ie}^{n} = \underline{C}_n^{b}(\underline{I}+\underline{E}^{n})\underline{\omega}_{ie}^{n}$$

where $\underline{E}$ is the skew symmetric error angle matrix.
Thus Eq. (1.14) becomes:

$$\underline{\omega}_{n'b}^{b} = \underline{\omega}_{cmd}^{b} + \underline{\omega}_{d}^{b} + (u)\underline{\omega}^{b} - \underline{E}^{b} \, \underline{\omega}_{ie}^{b} \tag{1.15}$$

The differential equation relating $\dot{\underline{E}}$ to $\underline{\omega}_{cmd}$ is found by substituting the skew symmetric form of equation (1.15) into equation (1.12)

$$\dot{\underline{C}}_b^{n'} = \underline{C}_b^{n'} \underline{\Omega}_{cmd}^b + \underline{C}_b^{n'} \underline{\Omega}_d^b + \underline{C}_b^{n'} (u)\underline{\Omega}^b - \underline{C}_b^{n'} \delta\underline{\Omega}_{ie}^b \tag{1.16}$$

where

$\delta\underline{\Omega}_{ie}^b$ is the skew symmetric form of $\underline{E}^b \underline{\omega}_{ie}^b$

Noting that:

$$\dot{\underline{C}}_b^{n'} = \underline{C}_n^{n'} \dot{\underline{C}}_b^n + \dot{\underline{C}}_n^{n'} \underline{C}_b^n \tag{1.17}$$

and

$$\dot{\underline{C}}_b^n = \underline{C}_b^n \underline{\Omega}_d^b , \tag{1.18}$$

equation (1.16) becomes:

$$\dot{\underline{C}}_n^{n'} \underline{C}_b^n = \underline{C}_b^{n'} \underline{\Omega}_{cmd}^b + \underline{C}_b^{n'} (u)\underline{\Omega}^b - \underline{C}_b^{n'} \delta\underline{\Omega}_{ie}^b \tag{1.19}$$

but $\dot{\underline{C}}_n^{n'} = - \dot{\underline{E}}^n$

Thus

$$\dot{\underline{E}}^n = - \underline{C}_b^{n'} \underline{\Omega}_{cmd}^b \underline{C}_n^b - \underline{C}_b^{n'} (u)\underline{\Omega}^b \underline{C}_n^b + \underline{C}_b^{n'} \delta\underline{\Omega}_{ie}^b \underline{C}_n^b$$

or

$$\dot{\underline{E}}^n = - \underline{\Omega}_{cmd}^n - (u)\underline{\Omega}^n + \delta\underline{\Omega}_{ie}^n \tag{1.20}$$

where, as usual, products of small quantities were neglected. We can write Eq. (1.20) in vector form:

$$\dot{\underline{\varepsilon}}^n = - \underline{\omega}_{cmd}^n - (u)\underline{\omega}^n - \underline{\Omega}_{ie}^n \underline{\varepsilon}^n , \tag{1.21}$$

since

$$- \underline{E}^n \underline{\omega}_{ie}^n = \underline{\Omega}_{ie}^n \underline{\varepsilon}^n$$

In order to drive $\underline{\varepsilon}^n$ to zero, $\underline{\omega}_{cmd}^n$ can be chosen to be a linear function of the measured estimate of $\underline{\varepsilon}^n$. We therefore choose:

$$\underline{\omega}_{cmd}^n = \underline{K} \underline{\varepsilon}_c^n \tag{1.22}$$

where

$\underline{K}$ ∿ 3 x 3 matrix to be specified

$\underline{\varepsilon}_c^n$ ∿ computed error vector

Thus equation (1.21) becomes:

$$\dot{\underline{\varepsilon}}^n + \underline{\Omega}_{ie}^n \, \underline{\varepsilon}^n + \underline{K} \, \underline{\varepsilon}_c^n = - \, (u)\underline{\omega}^n \tag{1.23}$$

Note that equation (1.23) represents three scalar differential equations which are coupled through the term $\underline{\Omega}_{ie}^n \, \underline{\varepsilon}^n$, which represents Earth rate coupling.

The elements of $\underline{\varepsilon}_c^n$ in equation (1.23) remain to be specified. A direct indication of the three components can be obtained from the computed horizontal components of $\underline{g}$ and the computed east component of $\underline{\omega}_{ie}$. Specifically, since

$$\underline{f}_c^{n'} = (\underline{I} - \underline{E}^n)\underline{f}_c^n$$

$$= (\underline{I} - \underline{E}^n)(- \underline{g}^n + \underline{f}_d^n + (u)\underline{f}^n)$$

and

$$\underline{g}^n = \{0, \; 0, \; g\}$$

then

$$f_{N_c} = g \; \varepsilon_E + f_{d_N} + (u)f_N \tag{1.24}$$

$$f_{E_c} = - \, g \; \varepsilon_N + f_{d_E} + (u)f_E \tag{1.25}$$

where $f_{d_N}$ and $f_{d_E}$ are the north and east components of the disturbance specific force vector and $(u)f_N$ and $(u)f_E$ are the north and east components of the accelerometer uncertainties, respectively. The remaining element, $\varepsilon_{D_c}$, is found by examining the expression for $\underline{\omega}_c$. From Figure 1.3,

$$\underline{\omega}_c^{n'} = \underline{C}_b^{n'}(\underline{\omega}_{ie}^b + \underline{\omega}_d^b + (u)\underline{\omega}^b)$$

$$= (\underline{I} - \underline{E}^n)\underline{C}_b^n(\underline{\omega}_{ie}^b + \underline{\omega}_d^b + (u)\underline{\omega}^b)$$

$$= (\underline{I} - \underline{E}^n)\underline{\omega}_{ie}^n + \underline{\omega}_d^n + (u)\underline{\omega}^n \tag{1.26}$$

The east component of the above equation is given by:

$$\omega_{E_c} = - \omega_{ie} \cos L \, (\varepsilon_D + \tan L \, \varepsilon_N) + \omega_{d_E} + (u)\omega_E \tag{1.27}$$

where $\omega_{d_E}$ and $(u)\omega_E$ are the east components of the disturbance angular velocity and gyro uncertainty, respectively.

The system is designed to process the $f_{N_c}$, $f_{E_c}$, and $\omega_{E_c}$ measurements assuming that there are no error sources.

$$\underline{\varepsilon}_c^n = \{ - \frac{f_{E_c}}{g}, \frac{f_{N_c}}{g}, \tan L \frac{f_{E_c}}{g} - \sec L \frac{\omega_{E_c}}{\omega_{ie}} \} \tag{1.28}$$

The error in the estimation, $\delta\underline{\varepsilon}$, is found by substituting

$$\underline{\varepsilon}_c = \underline{\varepsilon} + \delta\underline{\varepsilon}$$

and Eqs. (1.24), (1.25) and (1.27) into Eq. (1.28):

$$\underline{\varepsilon}_c^n = \underline{\varepsilon}^n + \delta\underline{\varepsilon}^n = \underline{\varepsilon}^n + \begin{bmatrix} - \frac{1}{g} (f_{d_E} + (u)f_E) \\ \frac{1}{g} (f_{d_N} + (u)f_N) \\ \frac{\tan L}{g} (f_{d_E} + (u)f_E) - \frac{\sec L}{\omega_{ie}} (\omega_{d_E} + (u)\omega_E) \end{bmatrix} \tag{1.29}$$

It is now necessary to determine the form of the $\underline{K}$ matrix used to drive the error angles to zero. One can use Kalman filtering techniques to determine the elements of $\underline{K}$. The determination of $\underline{K}$ is formulated in this manner in Ref. 11. We shall choose an easier method which will illustrate the important concepts but which will fall short of the "optimal" method. We shall require that $\underline{K}$ be chosen such that Eq. (1.23) becomes uncoupled. This can be accomplished since $\underline{\omega}_{in}^n$ is constant at a given latitude. Thus we are choosing the off-diagonal terms of $\underline{K}$ equal to minus the corresponding terms of the skew symmetric matrix $\underline{\Omega}_{ie}^n$, i.e., choose:

$$\underline{K} = \begin{bmatrix} K_N & -\omega_{ie} \sin L & 0 \\ \omega_{ie} \sin L & K_E & \omega_{ie} \cos L \\ 0 & -\omega_{ie} \cos L & K_D \end{bmatrix} \tag{1.30}$$

Thus Eq. (1.23) becomes:

$$\dot{\underline{\varepsilon}}^n + \underline{K}_d \, \underline{\varepsilon}^n + \underline{K} \, \delta\underline{\varepsilon}^n = - (u)\underline{\omega}^n \tag{1.31}$$

where

$\underline{K}_d \sim$ diagonal gain matrix (diagonal elements of Eq. 1.30)
$\delta\underline{\varepsilon} = \underline{\varepsilon}_c - \underline{\varepsilon} \sim$ estimation error for the error vector (defined by Eq. (1.29)

If the term $\underline{K} \, \delta\underline{\varepsilon}^n$ in Eq. (1.31) is examined in detail, it is seen that if the settling time of the system is to be reasonable,

$$K_N, \; K_E, \; K_D >> \omega_{ie}$$

Thus Eq. (1.31) is rewritten as:

$$\dot{\underline{\varepsilon}}^n + \underline{K}_d \, \underline{\varepsilon}^n = - (u)\underline{\omega}^n - \underline{K}_d \, \delta\underline{\varepsilon}^n \tag{1.32}$$

Equation (152) is a first order, uncoupled, vector differential equation for the error angles. The contributions from the various error sources is best seen by writing this equation in component form, where $p = \frac{d}{dt}$.

$$(p + K_N)\varepsilon_N = \frac{K_N}{g} (f_{d_E} + (u) f_E) - (u)\omega_N \tag{1.33a}$$

$$(p + K_E)\varepsilon_E = - \frac{K_E}{g} (f_{d_N} + (u) f_N) - (u)\omega_E \tag{1.33b}$$

$$(p + K_D)\varepsilon_D = K_D \left[ \frac{\sec L}{\omega_{ie}} (\omega_{d_E} + (u)\omega_E) - \frac{\tan L}{g} (f_{d_E} + (u) f_E) \right] - (u)\omega_D \tag{1.33c}$$

It is obvious by inspection of Eqs. (1.33) that this alignment scheme, in an analogous fashion to the physical acceleration coupled gyrocompass scheme, deteriorates at high latitudes,

becoming inoperative at the Earth's poles. Observe that the error angles are a function of both the base motion and the instrument uncertainty. The equations are readily solved using Laplace transform techniques. Assuming that the forcing functions are general functions of time, we have:

$$\bar{\varepsilon}_N = \frac{K_N}{g} \frac{(\bar{f}_{d_E} + (u)\bar{f}_E)}{s + K_N} - \frac{(u)\bar{\omega}_N}{s + K_N} + \frac{\varepsilon_N(0)}{s + K_N} \tag{1.34a}$$

$$\bar{\varepsilon}_E = -\frac{K_E}{g} \frac{(\bar{f}_{d_N} + (u)\bar{f}_N)}{s + K_E} - \frac{(u)\bar{\omega}_E}{s + K_E} + \frac{\varepsilon_E(0)}{s + K_E} \tag{1.34b}$$

$$\bar{\varepsilon}_D = \frac{K_D}{\omega_{ie}} \sec L \frac{(\bar{\omega}_{d_E} + (u)\bar{\omega}_E)}{s + K_D} - K_D \frac{\tan L}{g} \frac{(\bar{f}_{d_E} + (u)\bar{f}_E)}{s + K_D} - \frac{(u)\bar{\omega}_D}{s + K_D}$$

$$+ \frac{\varepsilon_D(0)}{s + K_D} \tag{1.34c}$$

Applying the convolution property:

$$\mathcal{L}^{-1} \frac{1}{s + K} \overline{\omega(s)} = \int_0^t e^{-K(t-\tau)} \omega(\tau)\, d\tau$$

The unique solution to Eqs. (1.34)for arbitrary inputs is given by:

$$\varepsilon_N(t) = e^{-K_N t} \int_0^t e^{K_N \tau} \left[\frac{K_N}{g} f_{d_E}(\tau) + \frac{K_N}{g} (u) f_E(\tau) - (u)\omega_N(\tau)\right] d\tau$$

$$+ \varepsilon_N(0)\, e^{-K_N t} \tag{1.35a}$$

$$\varepsilon_E(t) = e^{-K_E t} \int_0^t e^{K_E \tau} \left[-\frac{K_E}{g} f_{d_N}(\tau) - \frac{K_E}{g} (u) f_N(\tau) - (u)\omega_E(\tau)\right] d\tau$$

$$+ \varepsilon_E(0)\, e^{-K_E t} \tag{1.35b}$$

$$\varepsilon_D(t) = e^{-K_D t} \int_0^t e^{K_D \tau} \left\{ \frac{K_E}{\omega_{ie}} \sec L \left[ \omega_{d_E}(\tau) + (u)\omega_E(\tau) \right] \right.$$

$$\left. -K_D \frac{\tan L}{g} \left[ f_{d_E}(\tau) + (u) f_E(\tau) \right] - (u)\omega_D(\tau) \right\} d\tau + \varepsilon_D(0)\, e^{-K_D t} \qquad (1.35c)$$

Since the base motion is not specified, it will be best to treat Eqs. (1.35) statistically. We find the mean squared value by squaring Eqs. (1.35) and taking the mathematical expectation of the result. If the statistics of the independent variables are uncorrelated, i.e., if the various random processes are independent and if no more than one is biased, then the cross coupling terms will drop out when the mathematical expectation is taken. This laborious task is best left for computer solution.

We will investigate the system dynamics for the simple case of zero base motion, constant accelerometer uncertainty, and constant gyro uncertainty:

$$f_{d_E}(t) = f_{d_N}(t) = \omega_{d_E}(t) = 0$$

$$(u) f_k(t) = (u) f_k = \text{constant}, \quad k = N, E$$

$$(u)\omega_k(t) = (u)\omega_k = \text{constant}, \quad k = N, E, D$$

Eqs. (1.35) then yield:

$$\varepsilon_N = \left( \frac{(u) f_E}{g} - \frac{(u)\omega_N}{K_N} \right) (1 - e^{-K_N t}) + \varepsilon_N(0)\, e^{-K_N t} \qquad (1.36a)$$

$$\varepsilon_E = -\left( \frac{(u) f_N}{g} + \frac{(u)\omega_E}{K_E} \right) (1 - e^{-K_E t}) + \varepsilon_E(0)\, e^{-K_E t} \qquad (1.36b)$$

$$\varepsilon_D = \left( \frac{\sec L}{\omega_{ie}} (u)\omega_E - \tan L \frac{(u) f_E}{g} - \frac{(u)\omega_D}{K_D} \right) (1 - e^{-K_D t}) + \varepsilon_D(0)\, e^{-K_D t} \qquad (1.36c)$$

The steady state errors are seen to be given by:

$$\epsilon_{N_{ss}} = \frac{(u)f_E}{g} - \frac{(u)\omega_N}{K_N} \tag{1.37a}$$

$$\epsilon_{E_{ss}} = -\frac{(u)f_N}{g} - \frac{(u)\omega_E}{K_E} \tag{1.37b}$$

$$\epsilon_{D_{ss}} = \frac{\sec L}{\omega_{ie}}(u)\omega_E - \tan L \frac{(u)f_E}{g} - \frac{(u)\omega_D}{K_D} \tag{1.37c}$$

These equations are summarized in the following table:

| | $\epsilon_N$/ | $\epsilon_E$/ | $\epsilon_D$/ |
|---|---|---|---|
| /(u)$\omega_N$ | $-1/K_N$ | 0 | 0 |
| /(u)$\omega_E$ | 0 | $-1/K_E$ | $1/\omega_{ie}$ cos L |
| /(u)$\omega_D$ | 0 | 0 | $-1/K_D$ |
| /(u)$f_E$ | $1/g$ | 0 | -tan L/g |
| /(u)$f_N$ | 0 | $-1/g$ | 0 |

Figure 1.4 ∿ Analytic Gyrocompass Steady State Error Coefficients

Comparison with Ref. 1 which shows comparable information for an acceleration coupled physical gyrocompass reveals striking similarities between the two systems. Note that the primary error sources and sensitivities are the same for both systems. That is, the level errors are caused primarily by the accelerometer uncertainties and the azimuth error is caused primarily by the east gyro drift. It should be emphasized, however, that the effect of base motion is likely to be very significant in the alignment of a practical system, whether or not one uses a physical or analytic gyrocompass scheme.

## 1.4 Instrument Redundancy

Since the question of reliability in inertial navigation systems is often alluded to in technical literature, it is well to discuss certain aspects of the problem at this time. Although we could address ourselves to the reliability aspects of other components of the inertial navigation system, it has been found through experience that the gyros are the least reliable system components (Ref. 13). Thus we will consider various redundant gyro configurations.

To motivate the discussion, consider an I.M.U. with three gyros mounted with their input axes along three mutually orthogonal axes (triad configuration). Clearly the system will fail if any one gyro fails. If the gyros are assumed to fail independently and to follow an exponential failure rate, the reliability of such a system is given by the product of the reliabilities of the individual components:

$$R = e^{-3\lambda t} \tag{1.38}$$

where

$R \sim$ reliability $\sim$ probability that satisfactory performance will be attained for a specified time period

$\frac{1}{\lambda} \sim$ mean time to failure

$t \sim$ time

Thus to achieve a reliability of 0.95 for one year requires a gyro mean time to failure of 59 years. In a commercial application some consideration should be given to this aspect of system performance since a "cost of ownership" criterion is now being applied to inertial navigation system procurement.

If it has been established that gyro redundancy is required for a particular application, the problem still remains of choosing a gyro configuration which is optimal. This problem has

been studied by Gilmore (Ref 14). He finds that symmetric arrays yields optimal performance from a least squares weighting point of view and in addition yield maximum redundancy for the number of instruments in the particular array. Only three symmetrical arrays are shown to exist (a symmetrical array is defined by the placing of axes through the center of a sphere such that the great circle angles between the axes are equal). They are:

1. Triad ∿ axes normal to the faces of an angular hexahedron
2. Tetrad ∿ axes normal to the faces of a regular octahedron or tetrahedron
3. Hexad ∿ axes normal to the faces of a regular dodecahedron

The coordinate transformations between the tetrad and hexad configurations and the triad configuration are given by:

$$\underline{C}_{triad}^{tetrad} = \frac{\sqrt{3}}{3}\begin{bmatrix} 1 & 1 & 1 \\ -1 & 1 & 1 \\ -1 & -1 & 1 \\ 1 & -1 & 1 \end{bmatrix} \tag{1.39}$$

$$\underline{C}_{triad}^{hexad} = \begin{bmatrix} \sin\alpha & 0 & \cos\alpha \\ -\sin\alpha & 0 & \cos\alpha \\ \cos\alpha & \sin\alpha & 0 \\ \cos\alpha & -\sin\alpha & 0 \\ 0 & \cos\alpha & \sin\alpha \\ 0 & \cos\alpha & -\sin\alpha \end{bmatrix} \tag{1.40}$$

where

$\alpha$ ∿ one half the great circle angle between gyro input axes = 31° 48' 2.8"

Both the tetrad and hexad arrays are capable of effecting a solution if any three gyros are operating. Both systems have self-contained failure detection and isolation capability, an advantage over systems consisting of two redundant triads.

Having established the symmetric arrays as optimal, the task remains of computing the configuration reliabilities. If we take the tetrad as an example we see that the system will function if:

1. all four instruments operate
2. any combination of three instruments operate

Now the probability that all four will operate is given by (intersection of independent events):

$$P(4 \text{ operate}) = R^4 = e^{-4\lambda t} \tag{1.41}$$

while the probability that any combination of three will operate is given by:

$$P(3 \text{ operate}) = 4\ R^3(1-R) = 4\ e^{-3\lambda t}(1-e^{-\lambda t}) \tag{1.42}$$

then the configuration reliability is given by the sum of Eqs. (161) and (162) (union of mutually exclusive events):

$$R_{tetrad} = 4\ e^{-3\lambda t} - 3\ e^{-4\lambda t} \tag{1.43}$$

Similar reasoning can be used to how that the reliability for the hexad array is given by:

$$R_{hexad} = e^{-3\lambda t}(20 - 10\ e^{-3\lambda t} + 36\ e^{-2\lambda t} - 45\ e^{-\lambda t}) \tag{1.44}$$

Figure 1.5 shows plots of equations (1.38), (1.43) and (1.44). In addition, curves are shown for systems consisting of:

two redundant triads
three redundant triads
six orthogonal gyros
nine orthogonal gyros

The plots are made under the assumption that any failure can be detected and isolated. Note that the reliability of the non-orthogonal arrays is quite superior to that of the redundant orthogonal arrays.

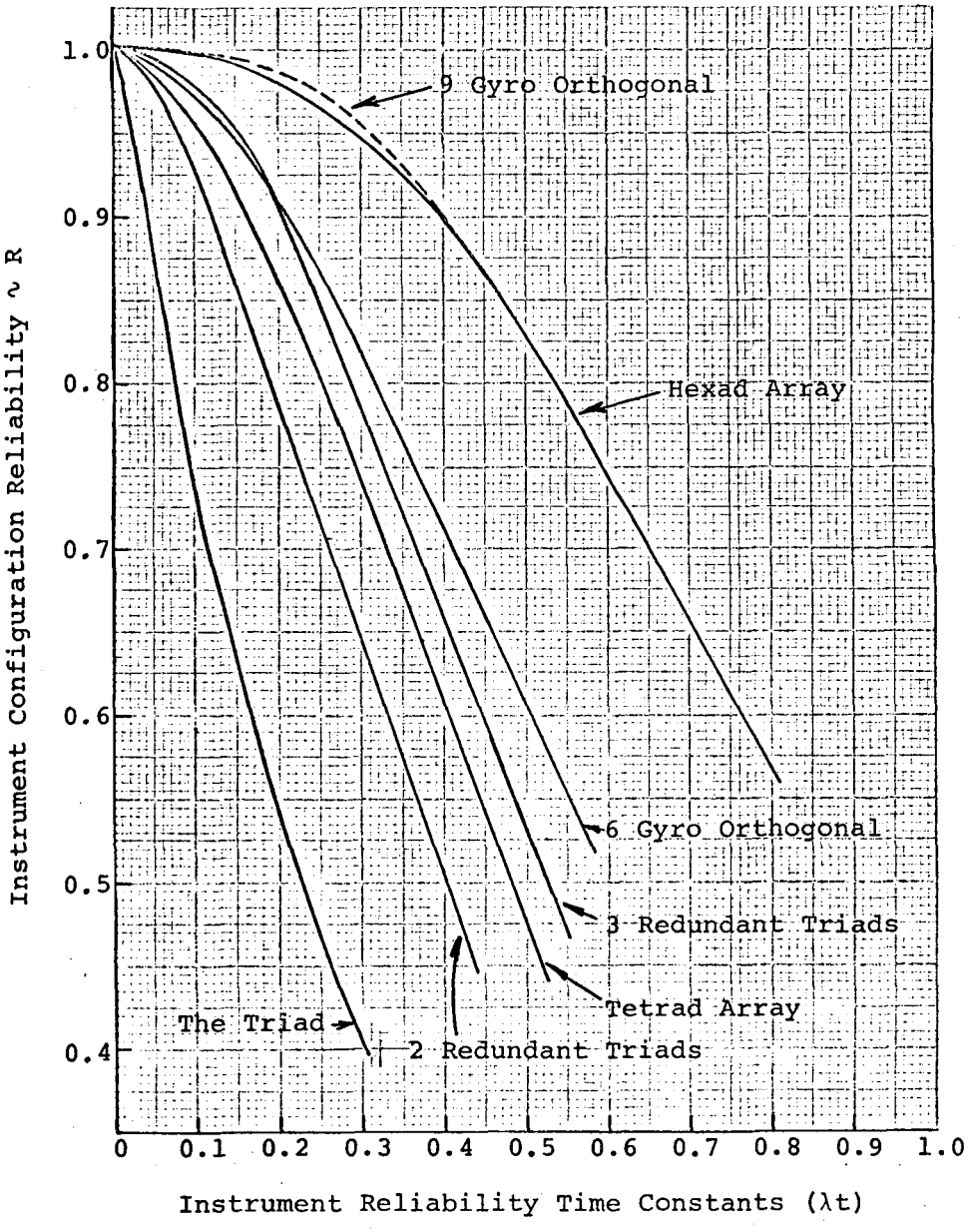


Fig.1.5 ∿ Reliability Plots - Perfect Failure Isolation

## 1.5 Error Analysis

In addition to the error sources treated for the gimbal systems which are considered in Section 2 the strapdown mechanization utilizing S.D.F. delta modulated rate gyros gives rise to several other error sources which must be modeled. A partial list of additional sources would include:

a. Gyro torquing asymmetry
b. Non-commutivity of the attitude matrices
c. Truncation error
d. Gyro and accelerometer quantization error
e. Computer round-off error

We first note from Fig. 1.2 that in the rate gyro mode the signal generator output, which is a voltage proportional to Ag, is affected by $\omega_{IA}$, Ag $\omega_{SRA}$, and $\dot{\omega}_{OA}$. The outputs which are proportional to Ag $\omega_{SRA}$ and $\dot{\omega}_{OA}$ must be compensated for if high accuracy is to be achieved. This is readily accomplished since $\omega_{OA}$ and $\omega_{SRA}$ are obtainable from the other gyros. Since all of the deterministic effects are hopefully accounted for, we model the residual as the uncertainty (u)$\underline{\omega}$.

### 1.5.1 Torquing Considerations

We have from Page 5 that the steady state equation relating the gyro output angle to the input axis angular velocity is given by:

$$(\omega_{ib})_c \simeq Ag = \omega_{IA}/\frac{\partial \omega_c}{\partial Ag}$$

where

$(\omega_{ib})_c \sim$ computed angular velocity

Thus, if the torquing scale factor, $\partial\omega_c/\partial Ag$, is not known precisely, the computed angular velocity along the gyro's input axis is in error by an amount given by:

$$(\omega_{ib})_c = \frac{\omega_{IA}}{\frac{\partial\omega_c}{\partial Ag} + \delta(\frac{\partial\omega_c}{\partial Ag})} = \frac{\omega_{IA}}{\partial\omega_c/\partial Ag}\,[1-\delta(\frac{\partial\omega_c}{\partial Ag})/(\frac{\partial\omega_c}{\partial Ag})]$$

$$\approx \omega_{IA} - \tau\,\omega_{IA}$$

where

$\tau = \delta(\frac{\partial\omega_c}{\partial Ag})/(\frac{\partial\omega_c}{\partial Ag})$ ∿ torquing scale factor uncertainty

Thus a positive scale factor error (scale factor too high) gives rise to a decrease in the measured angular rate.

In vector form we model the gyro scale factor error as:

$$\delta\underline{\omega}_T^b = -\,\underline{T}^b\,\underline{\omega}_{ib}^b \qquad (1.45)$$

where

$\delta\underline{\omega}_T$ ∿ error angular velocity in $\omega_{ib}$ due to torquing scale factor

$\underline{T}^b$ ∿ diagonal scale factor uncertainty matrix

$$= \begin{bmatrix} \tau_x & 0 & 0 \\ 0 & \tau_y & 0 \\ 0 & 0 & \tau_z \end{bmatrix}$$

Figure 1.6 shows a typical plot of measured angular rate versus true angular rate:

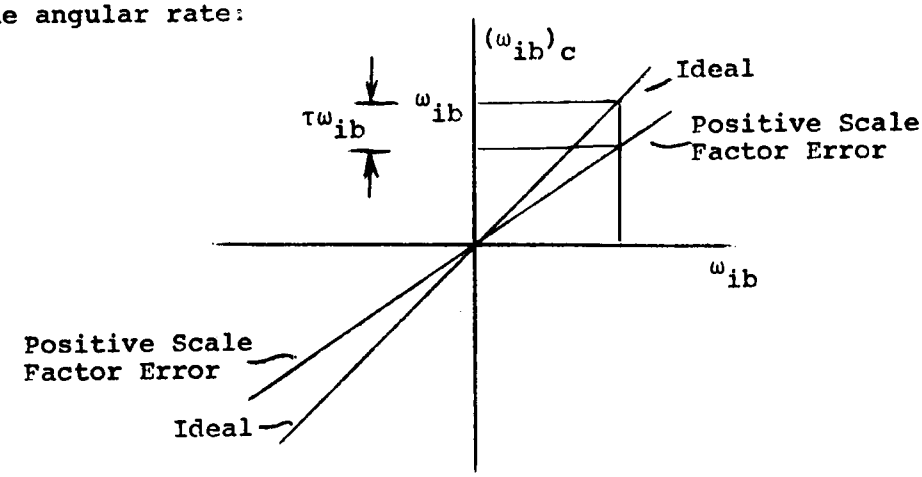


Fig. 1.6 ∿ Torquer Considerations

In a typical mission one does not sustain a constant angular velocity for indefinite periods. A typical angular vibration environment would result in the gyro operating in the null region. Note from Fig. 1.6 that a sinusoidal angular oscillation with a mean value equal to zero results in a zero mean angular velocity error equal to:

$$\delta\omega_T = - \tau\ \omega_{IA} \sin \omega\ t$$

where

$\omega_{IA}$ ∿ amplitude of input angular velocity
$\omega$ ∿ vibration frequency

If the scale factor error is asymmetric, however, sinusoidal angular vibrations can give rise to a growing error. Let us say that for positive inputs the scale factor error is given by $\tau^+$ and for negative inputs by $\tau^-$. Then for each cycle

$$\delta\theta_{T_a} = - \tau^+ \omega_{IA} \int_0^{\pi} \sin \omega\ t\ dt - \tau^- \omega_{IA} \int_{\pi}^{2\pi} \sin \omega\ t\ dt$$

$$= - 2\tau^+ \frac{\omega_{IA}}{\omega} + 2\tau^- \frac{\omega_{IA}}{\omega}$$

$$= 2 \frac{\omega_{IA}}{\omega} (\tau^- - \tau^+)$$

but for sinusoidal vibration, $\omega_{IA} = \theta\omega$,
where $\theta$ ∿ vibration amplitude.

$$\therefore \delta\theta_{T_a} = 2\ \theta\ (\tau^- - \tau^+) \qquad (1.46)$$

Thus for each vibration cycle an angular error results which is proportional to scale factor asymmetry. Let us evaluate an example to see what the magnitude of this buildup might be: Let us say that the vehicle is vibrating at $\omega$ = 10 cps with an amplitude of 1 $\widehat{\text{min}}$. Thus if we assume that $(\tau^- - \tau^+) = 10^{-5}$, the per cycle angular error is:

$$\delta\theta_{T_a} = 2 \times 10^{-5} \frac{\widehat{\text{min}}}{\text{cycle}}$$

For a two-hour flight, the accumulated error is equal to:

$$(\delta\theta_{T_a})_{2\ hr} = 2 \times 10^{-5} \frac{\widehat{min}}{cycle} \times 10 \frac{cycle}{sec} \times 2\ hr \times \frac{3600\ sec}{hr}$$

$$\approx 1.44\ \widehat{min}$$

This effect would appear to be quite significant and probably requires that the designer make a detailed evaluation of the angular vibration environment. In a particularly severe case, shock mounting would probably have to be employed. For a constant sinusoidal vibration along each gyro input axis, Eq. (166) in vector form can be expressed as an angular velocity uncertainty:

$$\delta\underline{\omega}_{T_a} = 2 \begin{bmatrix} (\tau_x^- - \tau_x^+)\theta_x & 0 & 0 \\ 0 & (\tau_y^- - \tau_y^+)\theta_y & 0 \\ 0 & 0 & (\tau_z^- - \tau_z^+)\theta_z \end{bmatrix} \underline{\omega}^b \qquad (1.47)$$

where

$\theta_k \sim$ vibration amplitude about $k^{th}$ gyro axis.

$\underline{\omega}^b \sim$ vibration frequency.

Obviously, for Eq. (1.47) to be used effectively, the angular vibration spectrum must be known. This type of data is rather scarce for any aircraft and, in addition, would tend to be strongly influenced by the aircraft type, mission, I.M.U. location, etc.

### 1.5.2 Commutation Error

Non-commutivity effects result from the fact that the attitude matrix computer is working with finite size angular outputs from the rate gyros. Thus an error will be introduced into the attitude matrix, $\underline{C}_b^n$. To investigate the form of this error, consider the case of three successive rotations about the body's positive x, y, and z axes. Then the coordinate transformation relating the rotated coordinates to the original body coordinates is given by:

$$\underline{C}_{b'}^{b} = \begin{bmatrix} \cos\theta_z & -\sin\theta_z & 0 \\ \sin\theta_z & \cos\theta_z & 0 \\ 0 & 0 & 1 \end{bmatrix} \begin{bmatrix} \cos\theta_y & 0 & \sin\theta_y \\ 0 & 1 & 0 \\ -\sin\theta_y & 0 & \cos\theta_y \end{bmatrix} \begin{bmatrix} 1 & 0 & 0 \\ 0 & \cos\theta_x & -\sin\theta_x \\ 0 & \sin\theta_x & \cos\theta_x \end{bmatrix}$$

where b' denotes the rotated frame.

If the rotation angles are equal to the $\Delta\theta$ pulse sizes, we can expand the above expression, keeping up to second order terms. We get an expression of the form:

$$\underline{C}_b^{b'} = (\underline{I} + \Delta\underline{\theta}^b)(\underline{I} + \underline{\Omega}^b) \tag{1.48}$$

where

$$\Delta\underline{\theta}^b = \begin{bmatrix} 0 & -\Delta\theta_z & \Delta\theta_y \\ \Delta\theta_z & 0 & -\Delta\theta_x \\ -\Delta\theta_y & \Delta\theta_x & 0 \end{bmatrix} \tag{1.49}$$

$$\underline{\Omega}^b = -\frac{1}{2} \begin{bmatrix} (\Delta\theta_y^2+\Delta\theta_z^2) & 0 & 0 \\ 0 & (\Delta\theta_x^2+\Delta\theta_z^2) & 0 \\ 0 & 0 & (\Delta\theta_x^2+\Delta\theta_y^2) \end{bmatrix} \tag{1.50}$$

The second order term represents the non-commutivity error. Thus a direct error results in the attitude matrix which is given by $-\underline{\Omega}_b$. Because this matrix is diagonal, the commutation error is seen to be similar to a scaling error. Also, from the symmetry of the above equation, it is seen that the form of the non-commutivity error is independent of the order of rotation. Since the commutation error is seen to be on the order of $\Delta\theta_k^2$, we choose the angle increments as small as possible consistent with computer speed and roundoff error considerations. Unfortunately, the prediction of the commutivity error with time requires a complete time history of the input angular velocity. Farrell (Ref. 12) has evaluated the error buildup in response to angular oscillations and finds the commutation error to be quite significant if the $\Delta\theta$ pulse sizes are not kept below about 20 $\widehat{\text{sec}}$. Systems are currently being built with pulse sizes in the 1 → 2 $\widehat{\text{sec}}$ range.

### 1.5.3 Truncation Error

As was pointed out in Section 1.2 truncation error results from approximations in the algorithm used to update the attitude matrix. From Eq. (1.9) the truncation error for the rectangular integration scheme is given by:

$$\delta\underline{C} = \frac{1}{2}\,\underline{C}(\underline{\Omega}^2 + \dot{\underline{\Omega}})\Delta t^2$$

This error is seen to be proportional to $(\Delta\theta)^2$. Thus it would appear that the truncation error might be reduced by using higher order integration schemes. This is indeed the case, but one must pay the penalty of more computation and more roundoff error for a given computer word length. The use of a high order iteration scheme results in the truncation error being insignificant in comparison with the commutation error discussed previously.

### 1.5.4 Quantization Error

Quantization error, which is to be distinguished from commutation error, is defined to be the error which results from the digital measurement and conversion of continous physical quantities such as the angular position of a gyro float assembly. These errors can result in at most one bit of information being lost during the mission. Treated statistically, the resulting error appears in the form of a random phase shift. Thus, by appropriate choice of quantization levels, the resulting navigation error can be reduced to negligible proportions.

Quantization effects become very important during alignment, however. It is readily seen that for the case of fixed base alignment the pulse rate is likely to be very low. Thus long filtering times are necessary to smooth the data. In addition, complications can be introduced by instruments which limit cycle because they are being pulse torqued (Ref. 9).

### 1.5.5 Roundoff Error

Roundoff error is associated with finite computer word length. Each time a computation is performed, the computer must approximate the last digit. This effect is readily analyzed using statistical methods to determine the word length required to yield a specified rms error after a specified number of computer iterations.

### 1.5.6 Orthogonalization

There is no guarantee that after many iterations, the computed attitude matrix will satisfy the orthogonality relationship:

$$\underline{C}^T \underline{C} = \underline{I}$$

It is readily seen that the errors resulting from commutation and truncation will result in a skewing of the computed reference axes. Although Ref. 12 shows that the periodic orthogonalization does not improve the attitude reference system performance, the

orthogonalization procedure is recommended for the purposes of analysis.

The attitude matrix can be orthogonalized by setting:

$$\underline{C}^* = \underline{C}(\underline{C}^T \underline{C})^{-1/2} \tag{1.51}$$

where

$\underline{C}^*$ ∿ optimal orthogonal approximation to $\underline{C}$ in the sense that trace $\{(\underline{C}^* - \underline{C})^T(\underline{C}^* - \underline{C})\}$ is minimized.

Unfortunately, there are no general rules which can be applied in determining the square root of a matrix· in fact, one cannot even predict how many roots exist. A solution, albeit non-unique, is readily generated using a computer.

## 1.5.7 Derivation of Error Equations

A strapdown system which computes in geographic coordinates will be analyzed in this section. The functional diagram for such a system is shown in Fig. 1.7.

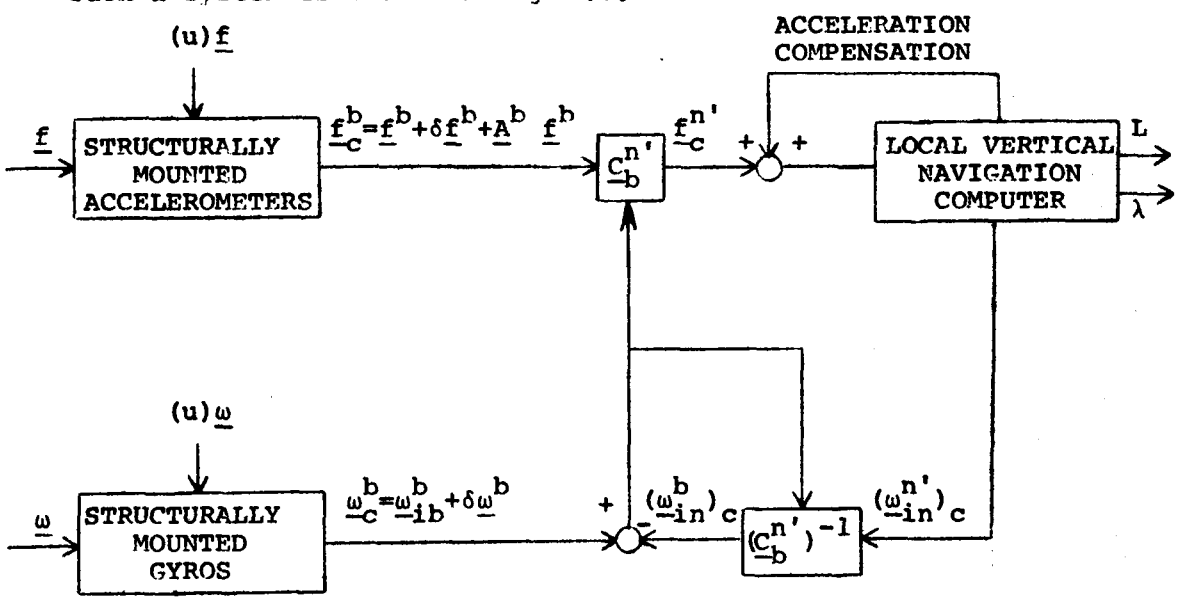


Fig. 1.7 ∿ Strapdown System Computing in Geographic Coordinates.

Note that in Fig.1.7 we have arbitrarily chosen to express the error in the transformation matrix as:

$$\underline{C}_b^{n'} = \underline{C}_n^{n'} \underline{C}_b^n = (\underline{I} - \underline{E}^n)\underline{C}_b^n$$

We could have proceeded to define the attitude matrix as:

$$\underline{C}_{b'}^n = \underline{C}_b^n \underline{C}_{b'}^b = \underline{C}_b^n(\underline{I} + \underline{E}^b)$$

which would, of course, vield identical results.

It is, of course, tacitly assumed that the attitude matrix, $\underline{C}_b^{n'}$, has been suitably orthogonalized per the method of Section 1.5.6 The attitude matrix is updated using the first order matrix equation:

$$\dot{\underline{C}}_b^{n'} = \underline{C}_b^{n'} \underline{\Omega}_{n'b}^b \tag{1.52}$$

Because of the orthogonalization procedure, the coordinate transformation relating the geographic coordinates to the computed geographic coordinates is given by:

$$\underline{C}_n^{n'} = \underline{I} - \underline{E}^n \tag{1.53}$$

where

$$\underline{E}^n = \begin{bmatrix} 0 & -\varepsilon_D & \varepsilon_E \\ \varepsilon_D & 0 & -\varepsilon_N \\ -\varepsilon_E & \varepsilon_N & 0 \end{bmatrix}$$

If we assume that all of the errors involved in computing the attitude matrix which were discussed previously can be treated as resulting from erroneous angular velocity command, the angular velocity used to update the matrix is given by:

$$\underline{\omega}_{n'b}^b = (\underline{\omega}_{ib}^b)_c - (\underline{C}_b^{n'})^{-1} (\underline{\omega}_{in}^{n'})_c \tag{1.54}$$

where

$(\underline{\omega}^b_{ib})_c$ ∿ computed angular velocity of the body coordinates with respect to inertial coordinates.

$(\underline{\omega}^n_{in})_c$ ∿ computed angular velocity of the geographic coordinates with respect to inertial coordinates.

Because of the uncertainties in the gyros and in the computation of $\underline{C}^{n'}_b$, the computed angular velocity is given by:

$$\underline{\omega}^b_{n'b} = \underline{\omega}^b_{ib} + \delta\underline{\omega}^b - \underline{C}^b_n \, \underline{C}^n_{n'} \, (\underline{\omega}^{n'}_{in})_c \tag{1.55}$$

where

$\delta\underline{\omega}^b$ ∿ equivalent angular velocity uncertainty which results from the various error sources.

But expansion of $(\underline{\omega}^{n'}_{in})_c$ shows that:

$$(\underline{\omega}^{n'}_{in})_c = \underline{\omega}^n_{in} + \underline{W}^n \, \underline{\omega}^n_{in}$$

where

$$\underline{W}^n = \begin{bmatrix} \frac{\delta\dot{\lambda}}{\dot{\lambda}} & 0 & \delta L \\ 0 & \frac{\delta\dot{L}}{\dot{L}} & 0 \\ -\delta L & 0 & \frac{\delta\dot{\lambda}}{\dot{\lambda}} \end{bmatrix}$$

Thus Eq. (1.55) becomes:

$$\underline{\omega}^b_{n'b} = \underline{\omega}^b_{ib} + \delta\underline{\omega}^b - \underline{C}^b_n(\underline{I} + \underline{E}^n)(\underline{I} + \underline{W}^n)\underline{\omega}^n_{in}$$

or

$$\underline{\omega}^b_{n'b} = \underline{\omega}^b_{nb} + \delta\underline{\omega}^b - (\underline{E}^b + \underline{W}^b)\underline{\omega}^b_{in} \tag{1.56}$$

Substituting the skew symmetric form of Eq. (1.56) into Eq. (1.52) yields:

$$\dot{\underline{C}}^{n'}_b = \underline{C}^{n'}_b (\underline{\Omega}^b_{nb} + \delta\underline{\Omega}^b - \delta\underline{\Omega}^b_{in}) \tag{1.57}$$

where

$\delta\underline{\Omega}^b_{in} \sim$ skew symmetric form of $(\underline{E}^b + \underline{W}^b)\underline{\omega}^b_{in}$

but

$$\dot{\underline{C}}^{n'}_b = \frac{d}{dt}(\underline{C}^{n'}_n \underline{C}^n_b) = \dot{\underline{C}}^{n'}_n \underline{C}^n_b + \underline{C}^{n'}_n \dot{\underline{C}}^n_b$$

$$= \underline{C}^{n'}_n \underline{\Omega}^n_{n'n} \underline{C}^n_b + \underline{C}^{n'}_n \underline{C}^n_b \underline{\Omega}^b_{nb}$$

Thus,

$$\underline{\Omega}^n_{n'n} = \delta\underline{\Omega}^n - \delta\underline{\Omega}^n_{in}$$

which can be written in vector form as:

$$\dot{\underline{\varepsilon}}^n = -\delta\underline{\omega}^n + (\underline{E}^n + \underline{W}^n)\underline{\omega}^n_{in} \tag{1.58}$$

but $\underline{E}^n \underline{\omega}^n_{in} = -\underline{\Omega}^n_{in} \underline{\varepsilon}^n$

thus

$$\dot{\underline{\varepsilon}}^n + \underline{\Omega}^n_{in} \underline{\varepsilon}^n - \underline{W}^n \underline{\omega}^n_{in} = -\delta\underline{\omega}^n \tag{1.59}$$

Equation (1.59)is three equations in five unknowns as is readily seen by writing out in component form:

$$\dot{\varepsilon}_N + \dot{\lambda} \sin L\, \varepsilon_E - \dot{L}\, \varepsilon_D - \cos L\, \delta\dot{\lambda} + \dot{\lambda} \sin L\, \delta L = -\delta\omega_N \tag{1.60a}$$

$$\dot{\varepsilon}_E - \dot{\lambda} \sin L\, \varepsilon_N - \dot{\lambda} \cos L\, \varepsilon_D + \delta\dot{L} = -\delta\omega_E \tag{1.60b}$$

$$\dot{\varepsilon}_D + \dot{L}\, \varepsilon_N + \dot{\lambda} \cos L\, \varepsilon_E + \dot{\lambda} \cos L\, \delta L + \sin L\, \delta\dot{\lambda} = -\delta\omega_D \tag{1.60c}$$

Comparison with Eq. (2.28)reveals that this equation is identical to the corresponding equation obtained for the local vertical platform system.

The latitude and longitude errors are specified by examining the expression for the computed specific force. The computed specific force is given by:

$$\underline{f}^b_c = \underline{f}^b + \delta\underline{f}^b + \underline{A}^b \underline{f}^b \tag{1.61}$$

(See Eq. 2.5 for definitions.)

where, in this situation, the accelerometer frame is the body frame. The computed specific force is transformed into the computed geographic frame by the computed attitude matrix. Thus:

$$\underline{f}_C^{n'} = \underline{f}^n - \underline{E}^n \underline{f}^n + \delta \underline{f}^n + \underline{A}^n \underline{f}^n \tag{1.62}$$

where products of small quantities have been neglected as usual. The derivation that now follows is identical to the corresponding local vertical navigation system development. (See Section 2)

Expressions for the computed specific force components are first expressed as a function of the specific force and the latitude, longitude, and altitude errors. The result is Eqs.(2.16) and (2.17). The appropriate components of Eq. (1.62)are then substituted into Eqs.(2.16) and (2.17)yielding Eqs.(2.18) and (2.19).

Eqs. (2.18), (2.19) and (1.60)are then solved simultaneously for the state vector. The equation to be solved is given by:

$$\underline{N} \begin{bmatrix} \varepsilon_N \\ \varepsilon_E \\ \varepsilon_D \\ \delta L \\ \delta \lambda \end{bmatrix} = \begin{bmatrix} -\delta \omega_N \\ -\delta \omega_E \\ -\delta \omega_D \\ (u) f_N - (\ddot{L} + 2\dot{L}\, p)\delta h - \xi g + a_N f_N \\ (u) f_E - \cos L\, (\ddot{\lambda} + 2\dot{\lambda}\, p)\delta h + \eta g + \omega_E f_E \end{bmatrix} \tag{1.63}$$

where

$\underline{N}$ ∿ the left-hand side of Eq. (2.28)

$\delta \underline{\omega}^n$ ∿ uncertainty in the equivalent computed angular velocity of the geographic frame relative to the body frame due to all of the relevant error sources.

$(u)f_N$ ∿ equivalent north accelerometer uncertainty.

$(u)f_E$ ∿ equivalent east accelerometer uncertainty.

The solution of this equation will be identical to that of the local vertical platform system. Thus the error response curves shown in Section 2 are directly applicable.

## 2. Local Vertical Inertial Navigation System

### 2.1 Introduction

The local vertical inertial navigator is a semi-analytic system instrumenting the geographic coordinate frame. That is, the reference axes of the space integrator are commanded into alignment with the local north-east-down coordinate system. The system is composed of a three-axis space integrator, two accelerometers which are orthogonally mounted in the instrumented east and north directions, and a computer to perform the necessary navigational computations. Figure 2.1 shows a functional block diagram for this type of system. Note that three accelerometers are indicated although the vertical accelerometer is usually not present.

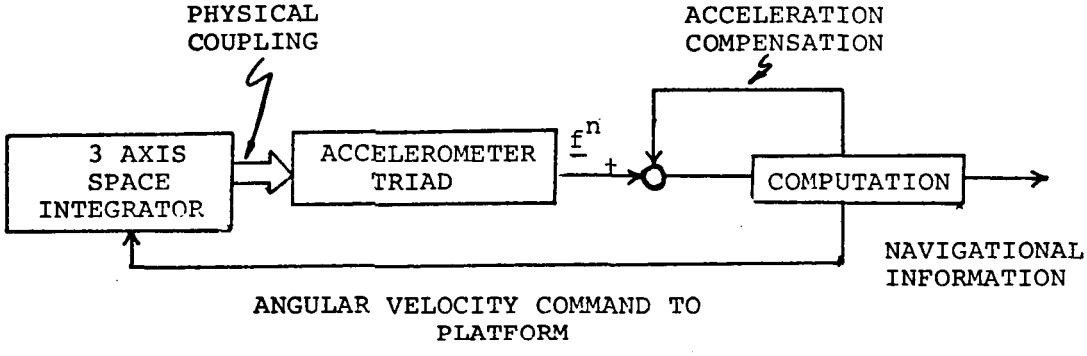


Figure 2.1. Local Vertical Inertial Navigation System

The instrumented north and east accelerometers are connected at the signal level with the east and north gyros, respectively. Since the vehicle carrying the navigation system may move freely over and above the surface of the earth, the space integrator gyros must be torqued at a rate proportional to vehicle longitude and latitude rate such that the platform can maintain its axes aligned with geographic axes. The required torquing signals are generated from the accelerometer outputs. Because the instrumented coordinate frame

is rotating with respect to inertial space, Coriolis terms are present in the accelerometer outputs. The accelerometer output signals must therefore be compensated such that gyro commands as a function of only longitude and latitude rates may be obtained. Note, however, that no explicit computation of the gravitational field is required since, neglecting the deflection of the vertical terms, the north and east accelerometers are nominally perpendicular to the gravity field vector, $\underline{g}$.

This configuration has an additional computational advantage in that no explicit coordinate transformations need be performed to obtain navigation information.

## 2.2 Description of System

The system design is motivated by examination of the expression for the non field specific force in navigational axes:

$$\underline{f}^n = \underline{C}_i^n [\ddot{\underline{r}}^i - \underline{G}^i] \qquad (2.1)$$

where

- $\underline{f}$ ∿ Nonfield specific force vector
- $\underline{r}$ ∿ Position vector from the center of the Earth to the system's location
- $\underline{G}$ ∿ Gravitational field vector
- $\underline{C}_i^n$ ∿ Coordinate transformation from inertial coordinates, "i", to geographic coordinates, "n".

Note that the superdot indicates a time differentation.

The geometry relating the geocentric inertial frame, "i", the geographic frame, "n"; and the geocentric earth frame, "e", is shown in Figure 2.2.

(N, E, D) ∿ Geographic

(x, y, z) ∿ Inertial

($x_e$, $y_e$, $z_e$) ∿ Earth

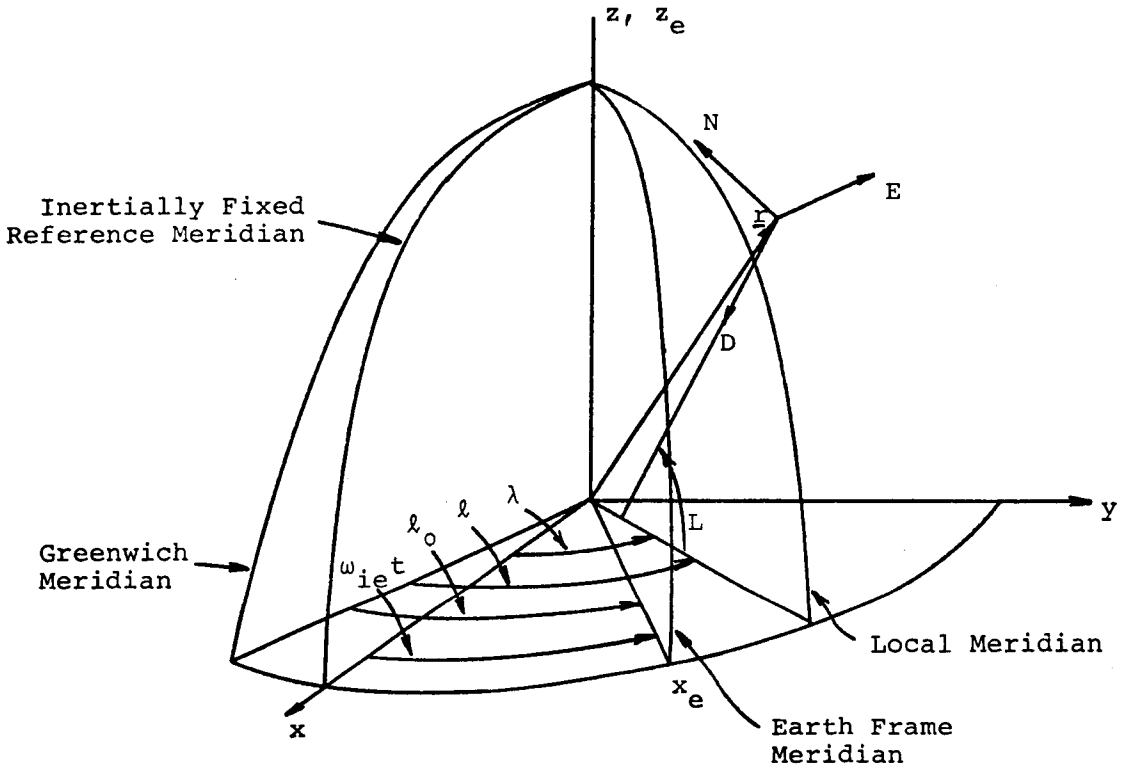


Figure 2.2. Coordinate Frame Geometry

In Figure 2.2,

$\ell$ ∿ Terrestrial longitude

$\lambda$ ∿ Celestial longitude

$\ell_o$ ∿ Reference longitude from Greenwich

L ∿ Geographic latitude

$\omega_{ie}$ ∿ Earth's angular velocity

Note also that at t = 0, the inertially fixed reference meridian, the earth frame meridian, and the local meridian are coincident. Thus we have that:

$$\lambda = \ell - \ell_o + \omega_{ie} t \tag{2.2}$$

Equation 2.1 can be written as a function of the geographic latitude, L, celestial longitude, $\lambda$, and the radii of curvature, $r_L$ and $r_\ell$ as follows:

$$\underline{f}^n = \begin{bmatrix} r_L \ddot{L} + \frac{1}{2} r_\ell (\dot{\lambda}^2 - \omega_{ie}^2) \sin 2L + 2\dot{r}_L \dot{L} + 2\frac{h}{r_o} \ddot{r} e \sin 2L - 3 e r \sin 2L \, \dot{L}^2 - \xi g \\ r_\ell \ddot{\lambda} \cos L - 2 r_\ell \dot{L} \dot{\lambda} \sin L + 2 \dot{r}_\ell \dot{\lambda} \cos L + \eta g \\ -g - \ddot{r} - r_L \ddot{L} e \sin 2L + r_\ell (\dot{\lambda}^2 - \omega_{ie}^2) \cos^2 L + \frac{r_L^2}{r} \dot{L}^2 \end{bmatrix} \tag{2.3}$$

where:

$r_L \cong r(1 - 2e \cos 2L)$

∿ radius of curvature in meridian plane

$r_\ell \cong r(1 + 2e \sin^2 L)$

∿ radius of curvature in co-meridian plane

$\xi$ ∿ meridian deflection of the vertical (positive about east)

$\eta$ ∿ prime deflection of the vertical (positive about north)

e ∿ earth's ellipticity ≅ 1/297

g ∿ magnitude of gravity

$r_o$ ∿ local geocentric earth radius magnitude

h ∿ height above reference earth model's surface

Equation 2.3 is an approximate expression which contains terms which are greater than $2 \times 10^{-5}$g for the following maximum values of vehicle motion:

$$r\ddot{L}_{max} = r\ddot{\lambda}_{max} \leq 0.5g$$

$$\dot{L}_{max} = \dot{\ell}_{max} \leq 2.2 \times 10^{-4} \text{ rad/sec}$$

$$\dot{r}_{max} \leq 100 \text{ ft/sec}$$

$$\ddot{r}_{max} \leq 2g$$

Those limits correspond to those which one would expect to encounter in an aircraft application such as the supersonic transport. See ref. 1 for the details of the derivation of eq. 2.3.

Navigational information is readily obtained from $\underline{f}^n$ since, if Coriolis and cross coupling compensation is provided in eq. 2.3, then

$$\underline{f}^n_{compensated} = \begin{bmatrix} r_L\ddot{L} - \xi g \\ r_\ell \ddot{\lambda} \cos L \\ -\ddot{r} - g \end{bmatrix}$$

Latitude and longitude can then be found by a double time integration of the north and east specific force measurements, respectively.

It is also necessary to generate the angular velocity command to the space integrator such that the geographic frame is instrumented. Since an uncommanded space integrator will remain nonrotating with respect to inertial space, the required torquing command is just the angular velocity of the geographic frame with respect to the inertial frame.

$$\underline{\omega}^{n}_{in} = \begin{bmatrix} \dot{\lambda} \cos L \\ -\dot{L} \\ -\dot{\lambda} \sin L \end{bmatrix} = \begin{bmatrix} (\omega_{ie} + \dot{\ell}) \cos L \\ -\dot{L} \\ -(\omega_{ie} + \dot{\ell}) \sin L \end{bmatrix} \tag{2.4}$$

Figure 2.3 illustrates the mechanization in detail.

In Figure 2.3 the subscript "c" denotes a computed physical quantity. In addition it was noted that the earth referenced velocity, coordinatized in geographic axes is given by (to an accuracy of better than 0.1 ft/sec for aircraft altitudes):

$$\underline{v}^{n} \cong \begin{bmatrix} r_L \dot{L} \\ r_\ell \dot{\ell} \cos L \\ -\dot{h} \end{bmatrix}$$

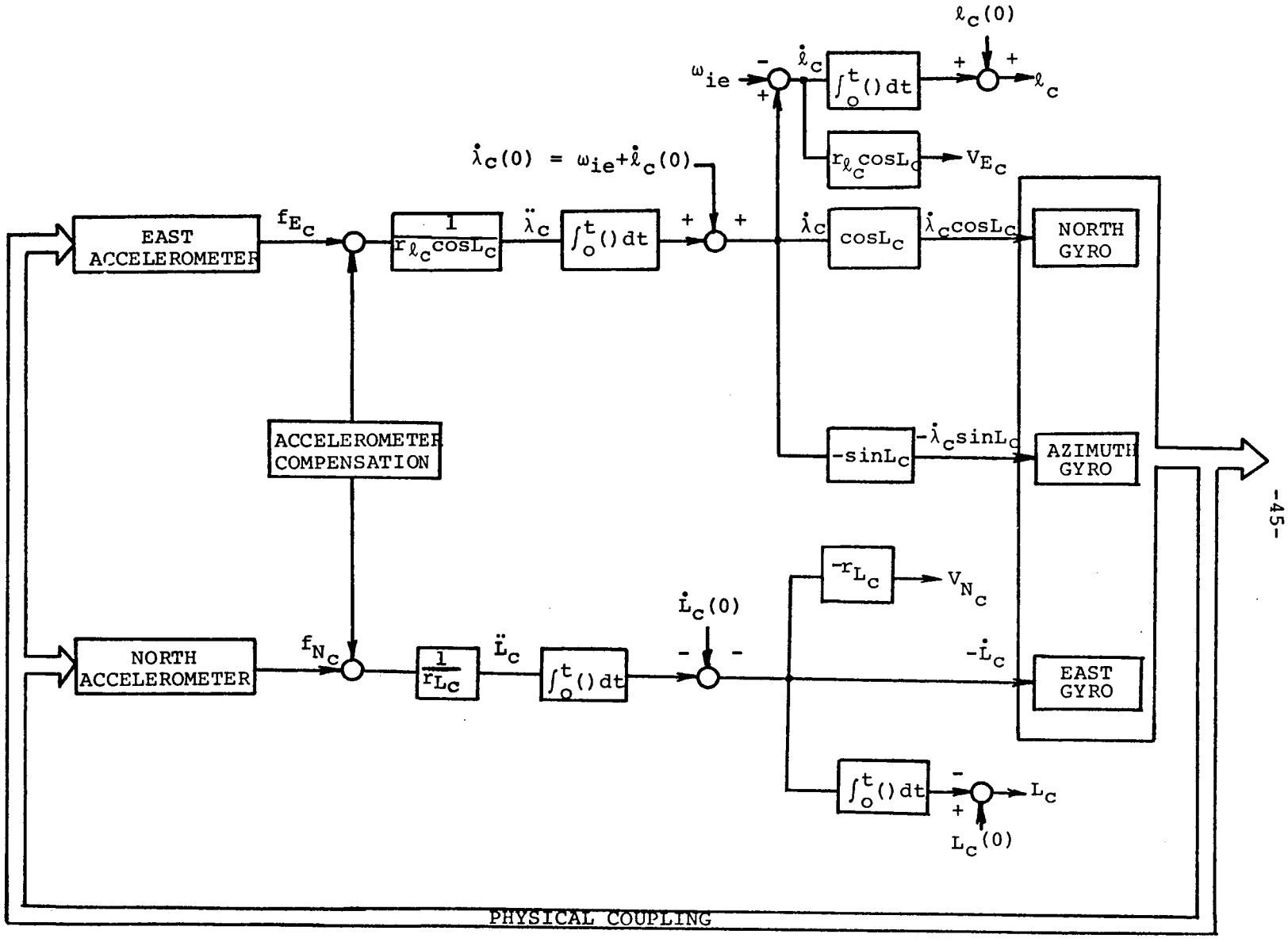


Figure 2.3 ∿ Local Vertical System Mechanization

## 2.3 Alignment

The alignment procedure for the local vertical inertial navigation system consists of physically aligning a coordinate frame associated with the inertial measurement unit with the geographic frame. If optical means are used for alignment, then fiducial lines on the platform representing the platform coordinate axes are aligned with geographic axes. The platform coordinates are then related to the gyro and accelerometer input axis coordinates through a calibration procedure. If on the other hand, gyrocompassing schemes are used for alignment, the gyro and accelerometer input axis coordinate system is physically aligned with the geographic coordinate system. For our purposes, we will assume that the relationship between the instrument axes and platform axes has been accurately determined through calibration procedures, allowing us to think of the platform frame as being synonymous with the frame defined by the instrument axes.

Reference 1 treats the case of fixed base physical gyrocompass alignment, while reference 2 looks at the effect of base motion on gyrocompass performance. In reference 3, a unified theory of alignment is developed. The subject of alignment will not be developed further in this report.

## 2.4 Error Analysis of Local Vertical System

The error equations will be developed using perturbation techniques for the following error sources:

gyro drift
gyro torquing uncertainty
accelerometer uncertainty and scale factor error
deflection of the vertical
initial platform misalignment
initial condition errors

The computed specific force, $\underline{f}$, is given by:

$$\underline{f}_c^p = \underline{f}^p + (u)\underline{f}^p + \underline{A}^p \underline{f}^p \qquad (2.5)$$

where

$(u)\underline{f}^p \sim$ accelerometer measurement uncertainty vector

$\underline{A}^p \sim$ accelerometer scale factor uncertainty matrix

$$\underline{A}^p = \begin{bmatrix} a_N & 0 & 0 \\ 0 & a_E & 0 \\ 0 & 0 & a_D \end{bmatrix}$$

and $a_k$, k = N,E,D is the scale factor uncertainty associated with the $k^{th}$ accelerometer, expressed as a numerical ratio. In this case, the accelerometer frame is the instrumented geographic frame denoted by "p" super/subscripts. The instrumented or platform axes differ from the true geographic axes because of imprecise torquing commands due to the error sources. If we define error angles $\varepsilon_N$, $\varepsilon_E$, and $\varepsilon_D$ resulting from positive rotations of the instrumented frame about positive geographic axes, then:

$$\underline{C}_p^n = \begin{bmatrix} 1 & -\varepsilon_D & \varepsilon_E \\ \varepsilon_D & 1 & -\varepsilon_N \\ -\varepsilon_E & \varepsilon_N & 1 \end{bmatrix} = [\underline{I} + \underline{E}^n] \qquad (2.6)$$

Thus:

$$\underline{f}_c^p = [\underline{I} - \underline{E}^n]\, \underline{f}^n + (u)\underline{f}^p + \underline{A}^p \underline{f}^p = \{f_{N_c}, f_{E_c}, f_{D_c}\} \qquad (2.7)$$

As is shown in Figure 2.3, the computation scheme assumes that the outputs of the north and east accelerometers are given by the north and east components of equation (2.3). Thus the indication of latitude and longitude is found by subtracting off the Coriolis and cross coupling terms from the components of equation (2.7). Thus

$$r_{L_c}\ddot{L}_c = f_{N_c} - \frac{1}{2} r_{\ell_c}(\dot{\lambda}_c^2 - \omega_{ie}^2)\sin 2L_c - 2\dot{r}_{L_c}\dot{L}_c - 2\frac{h_c}{r_{o_c}}\dot{r}_c e \sin 2L_c + 3e r_c \sin 2L_c \dot{L}_c^2 \quad (2.8)$$

$$r_{\ell_c}\ddot{\lambda}_c \cos L_c = f_{E_c} + 2r_{\ell_c}\dot{L}_c\dot{\lambda}_c \sin L_c - 2\dot{r}_{\ell_c}\dot{\lambda}_c \cos L_c \quad (2.9)$$

Note that the deflection of the vertical terms cannot be included in the above expression since no knowledge of their magnitudes is assumed. Writing out the expression for $f_{N_c}$ and $f_{E_c}$ from eq. (2.7):

$$f_{N_c} = f_N + \varepsilon_D f_E - \varepsilon_E f_D + (u) f_N + a_N f_N \quad (2.10)$$

$$f_{E_c} = f_E - \varepsilon_D f_N + \varepsilon_N f_D + (u) f_E + a_E f_E \quad (2.11)$$

Now the computed expressions for the radii of curvature are given by:

$$r_{L_c} = r_c(1 - 2e \cos 2L_c)$$

$$r_{\ell_c} = r_c(1 + 2e \sin^2 L_c)$$

But the calculated magnitude of the earth radius vector is given by:

$$r_c = r_{o_c} + h_c \quad (2.12)$$

where

$r_{o_c}$ ∿ calculated local geocentric earth radius magnitude

$\simeq r_e(1 - e \sin^2 L_c)$

$h_c$ ∿ estimated height above the reference earth model's surface

$r_e$ ∿ earth's equatorial radius

Substituting the following error quantities in eq. (2.12)

$$\delta L = L_c - L$$

$$\delta h = h_c - h$$

there results:

$$r_c \simeq r + \delta h \qquad (2.13)$$

where the small quantities involving products of e and error quantities have been neglected.

Thus

$$r_{L_c} = r[1 - 2e \cos 2(L + \delta L)] + \delta h$$

$$r_{\ell_c} = r[L + 2e \sin^2(L + \delta L)] + \delta h$$

or

$$r_{L_c} \simeq r_L + \delta h \qquad (2.14)$$

$$r_{\ell_c} \simeq r_\ell + \delta h \qquad (2.15)$$

If eqs. (2.10), (2.11), (2.13), (2.14), and (2.15) and the error quantities:

$$L_c = L + \delta L; \quad \lambda_c = \lambda + \delta\lambda$$

are substituted into eqs. (2.8) and (2.9), there results: (2.16)

$$r\ \ddot{\delta L} + r\ \dot{\lambda}\ \sin 2L\ \dot{\delta\lambda} = -\xi g + (u)f_N + a_N f_N + \varepsilon_D f_E - \varepsilon_E f_D - \ddot{L}\delta h - 2\dot{L}\ \dot{\delta h}$$

$$r\ \cos L\ \ddot{\delta\lambda} + 2(\dot{r}\ \cos L - r\ \dot{L}\ \sin L)\dot{\delta\lambda} - 2r\ \dot{\lambda}\ \sin L\ \dot{\delta L} - r(\ddot{\lambda}\ \sin L + 2\dot{L}\dot{\lambda}\cos L)\delta L =$$

$$\eta g + (u)f_E + a_E f_E + f_D\varepsilon_N - f_N\varepsilon_D - 2\ \dot{\lambda}\ \cos L\ \dot{\delta h} - \ddot{\lambda}\cos L\ \delta h \quad (2.17)$$

In deriving eqs. (2.16) and (2.17) only terms with magnitude greater than $2 \times 10^{-5}$g have been retained when the vehicle motion has the same maximum values assumed in the derivation of eq.(2.3) and if, in addition the following error data is specified.

$$\delta L_{max} = \delta\lambda_{max} = 10\ \widehat{min} = 2.9 \times 10^{-3}\ \text{rad}$$

$$\dot{\delta L}_{max} = \dot{\delta\lambda}_{max} = \delta L_{max}\omega_s = 3.6 \times 10^{-6}\ \text{rad/sec}$$

$$\ddot{\delta L}_{max} = \ddot{\delta\lambda}_{max} = \delta L_{max}\omega_s^2 = 4.5 \times 10^{-9}\ \text{rad/sec}^2$$

$$\delta h_{max} = 2000\ \text{ft.}$$

$$\dot{\delta h}_{max} = \delta h_{max}\omega_s = 2.5\ \text{ft/sec}$$

where $\omega_s = (g/r)^{1/2}$, is the Schuler frequency.

Substituting in the analytic expressions for the specific force components in the fε terms from eq. (2.3), neglecting terms with magnitude less than $2 \times 10^{-5}$g when:

$$\varepsilon_k < 10\ \widehat{min} = 2.9 \times 10^{-3}\ \text{rad},\ k = N, E, D$$

$$a_N\ \&\ a_E < 1/10^3$$

yields:

$$r\,\delta\ddot{L} + r\,\dot{\lambda}\sin 2L\,\delta\dot{\lambda} - (g + \ddot{r} - r\dot{\lambda}^2\cos^2 L - r\dot{L}^2)\varepsilon_E + r(2\dot{L}\,\dot{\lambda}\sin L - \ddot{\lambda}\cos L)\varepsilon_D =$$

$$-\xi g - \ddot{L}\,\delta h - 2\dot{L}\,\delta\dot{h} + (u)\,f_N + a_N\,r\ddot{L} \qquad (2.18)$$

$$r\cos L\,\delta\ddot{\lambda} + 2(\dot{r}\cos L - r\dot{L}\sin L)\,\delta\dot{\lambda} - 2r\,\dot{\lambda}\sin L\,\delta\dot{L} - r(\ddot{\lambda}\sin L + 2\dot{L}\dot{\lambda}\cos L)\delta L +$$

$$r(\ddot{L} + \tfrac{1}{2}\,\dot{\lambda}^2\sin 2L)\varepsilon_D + (g + \ddot{r} - r\,\dot{\lambda}^2\cos^2 L - r\dot{L}^2)\varepsilon_N =$$

$$\eta g - 2\,\dot{\lambda}\cos L\,\delta\dot{h} - \ddot{\lambda}\cos L\,\delta h + (u)\,f_E + a_E\,r\cos L(\ddot{\lambda} - 2\dot{L}\,\dot{\lambda}\tan L) \qquad (2.19)$$

Equations (2.18) and (2.19) are two equations in the five unknowns $\delta L$, $\delta\lambda$, $\varepsilon_N$, $\varepsilon_E$, and $\varepsilon_D$. Thus to specify the error behavior three additional equations are needed. These additional equations are found by examining the equations of motion for the gyro stabilized platform, or space integrator.

The angular velocity of the space integrator, i. e. the instrumented platform axes, with respect to the inertial frame:

$$\underline{\omega}^{p}_{ip} = \underline{C}^{p}_{n}\ \omega^{n}_{in} + \underline{\omega}^{p}_{np} \qquad (2.20)$$

is equal to the applied angular rate plus the gyro drift:

$$[\underline{I} + \underline{T}^{p}] \begin{bmatrix} \dot{\lambda}_c \cos L_c \\ -\dot{L}_c \\ -\dot{\lambda}_c \sin L_c \end{bmatrix} + \begin{bmatrix} (u)\omega_N \\ (u)\omega_E \\ (u)\omega_D \end{bmatrix} = [\underline{I} + \underline{T}^{p}]\underline{\omega}^{p}_{c} + (u)\underline{\omega}^{p} \qquad (2.21)$$

where

$L_c$ and $\lambda_c$ $\sim$ computed geographic latitude and celestial longitude, respectively.

$\underline{\omega}^{p}_{c}$ $\sim$ computed angular velocity command.

$$\underline{T}^{p} = \begin{bmatrix} \tau_N & 0 & 0 \\ 0 & \tau_E & 0 \\ 0 & 0 & \tau_D \end{bmatrix} \sim \text{torquing scale factor uncertainty matrix}$$

and

$(u)\underline{\omega}^{p}$ $\sim$ gyro drift vector.

$$= \{(u)\omega_N,\ (u)\omega_E,\ (u)\omega_D\}$$

Since computed latitude and longitude are given by:

$$L_c = L + \delta L$$

$$\lambda_c = \lambda + \delta\lambda$$

then:

$$\underline{\omega}_c^p = \underline{\omega}_{in}^n + \underline{W}^n \underline{\omega}_{in}^n \tag{2.22}$$

where

$$\underline{W}^n = \begin{bmatrix} \frac{\dot{\delta\lambda}}{\dot{\lambda}} & 0 & \delta L \\ 0 & \frac{\dot{\delta L}}{\dot{L}} & 0 \\ -\delta L & 0 & \frac{\dot{\delta\lambda}}{\dot{\lambda}} \end{bmatrix}$$

Finally, then

$$\begin{aligned} \underline{\omega}_{ip}^p &= \underline{\omega}_{in}^n + \underline{W}^n \underline{\omega}_{in}^n + \underline{T}^p \underline{\omega}_{in}^n + (u)\underline{\omega}^p \\ &= (\underline{I} + \underline{W}^n + \underline{T}^p) \underline{\omega}_{in}^n + (u) \underline{\omega}^p \end{aligned} \tag{2.23}$$

Equating equations (2.20) and (2.23) yields an expression for the error angles of the form:

$$(\underline{I} - \underline{E}^n) \underline{\omega}_{in}^n + \underline{\omega}_{np}^p = (\underline{I} + \underline{W}^n + \underline{T}^p) \underline{\omega}_{in}^n + (u) \underline{\omega}^p$$

which can be rearranged as:

$$\underline{\omega}_{np}^p = (\underline{W}^n + \underline{T}^p + \underline{E}^n) \underline{\omega}_{in}^n + (u) \underline{\omega}^p \tag{2.24}$$

The above equation is a first order linear vector differential equation with time varying coefficients, as can be readily seen by the writing out of the equation in component form:

$$\dot{\varepsilon}_N - \dot{L}\,\varepsilon_D + \dot{\lambda}\sin L\,\varepsilon_E = \cos L\;\delta\dot{\lambda} + \tau_N\,\dot{\lambda}\cos L - \dot{\lambda}\sin L\,\delta L + (u)\omega_N \tag{2.25}$$

$$\dot{\varepsilon}_E - \dot{\lambda}\cos L\,\varepsilon_D - \dot{\lambda}\sin L\,\varepsilon_N = -\delta\dot{L} - \tau_E\,\dot{L} + (u)\,\omega_E \tag{2.26}$$

$$\dot{\varepsilon}_D + \dot{\lambda}\cos L\,\varepsilon_E + \dot{L}\,\varepsilon_N = -\dot{\lambda}\cos L\,\delta L - \sin L\;\delta\dot{\lambda} - \tau_D\;\dot{\lambda}\sin L + (u)\omega_D \tag{2.27}$$

Equations (2.18), (2.19), (2.25), (2.26), and (2.27) are the required five equations in five unknowns which specify the platform error angles and the latitude and longitude errors. Using the differential operator $p = \frac{d}{dt}$, these equations can be arranged in matrix form as follows:

$$
\begin{bmatrix}
p & \dot{\lambda}\sin L & -\dot{L} & \dot{\lambda}\sin L & -\cos L\, p \\
-\dot{\lambda}\sin L & p & -\dot{\lambda}\cos L & p & 0 \\
\dot{L} & \dot{\lambda}\cos L & p & \dot{\lambda}\cos L & \sin L\, p \\
0 & \begin{matrix}-g - \ddot{r} + r\dot{L}^2 \\ +r\,\dot{\lambda}^2\cos^2 L\end{matrix} & \begin{matrix}2r\,\dot{L}\,\dot{\lambda}\sin L \\ -r\,\ddot{\lambda}\cos L\end{matrix} & r\,p^2 & r\,\dot{\lambda}\sin 2L\, p \\
\begin{matrix}g + \ddot{r} - r\dot{L}^2 \\ -r\,\dot{\lambda}^2\cos^2 L\end{matrix} & 0 & \begin{matrix}r(\ddot{L} + \\ \frac{1}{2}\dot{\lambda}^2\sin 2L)\end{matrix} & \begin{matrix}-2r(\dot{\lambda}\sin L\, p + \\ \dot{L}\,\dot{\lambda}\cos L + \\ \frac{1}{2}\ddot{\lambda}\sin L)\end{matrix} & \begin{matrix}(r\cos L\, p + \\ 2\dot{r}\cos L - \\ 2r\,\dot{L}\sin L)\, p\end{matrix}
\end{bmatrix}
\begin{bmatrix} \epsilon_N \\ \epsilon_E \\ \epsilon_D \\ \delta L \\ \delta\lambda \end{bmatrix}
=
$$

$$\begin{bmatrix} (u)\ \omega_N + \tau_N\ \dot{\lambda}\ \cos L \\ (u)\ \omega_E - \tau_E\ \dot{L} \\ (u)\ \omega_D - \tau_z\ \dot{\lambda}\ \sin L \\ (u)\ f_N + a_N\ r\ddot{L} - \xi g - (\ddot{L} + 2\dot{L}\ p)\ \delta h \\ (u)\ f_E + a_E\ r\cos L\ (\ddot{\lambda} - 2\ \dot{L}\ \dot{\lambda}\ \tan L) + \eta g - \cos L\ (\ddot{\lambda} + 2\ \dot{\lambda}\ p)\ \delta\ h \end{bmatrix} \qquad (2.28)$$

Solution of the matrix equation (2.28) will give the error response for the local vertical inertial navigator for arbitrary vehicle motion within the constraints stated. Analytic solution of the equation (2.28) would be quite tedious since the coefficients of the matrix equation are time varying except for the case of constant celestial longitude rate, $\dot{\lambda}$ = constant, and constant latitude, L = constant.

Considerable simplification occurs if we examine the stationary case where:

$$\ddot{L} = \ddot{\lambda} = \ddot{r} = \dot{r} = \dot{L} = 0; \quad \dot{\lambda} = \omega_{ie},$$

giving:

$$\begin{bmatrix} p & \omega_{ie}\sin L & 0 & \omega_{ie}\sin L & -\cos L\, p \\ -\omega_{ie}\sin L & p & -\omega_{ie}\cos L & p & 0 \\ 0 & \omega_{ie}\cos L & p & \omega_{ie}\cos L & \sin L\, p \\ 0 & -g & 0 & r\, p^2 & r\omega_{ie}\sin 2L\, p \\ g & 0 & 0 & -2r\omega_{ie}\sin L\, p & r\cos L\, p^2 \end{bmatrix} \begin{bmatrix} \varepsilon_N \\ \varepsilon_E \\ \varepsilon_D \\ \delta L \\ \delta\lambda \end{bmatrix}$$

$$= \begin{bmatrix} (u)\omega_N + \tau_N\, \omega_{ie}\cos L \\ (u)\omega_E \\ (u)\omega_D - \tau_D\, \omega_{ie}\sin L \\ (u)f_N - \xi g \\ (u)f_E + \eta g \end{bmatrix} \qquad (2.29)$$

Note that the $2 \times 10^{-5}$g criteria must again be applied in obtaining eq. (2.29) from eq. (2.28).

Initial condition errors, $\delta L(0)$, $\dot{\delta L}(0)$, $\delta\lambda(0)$, $\dot{\delta\lambda}(0)$, and initial misalignment errors, $\varepsilon_N(0)$, $\varepsilon_E(0)$, $\varepsilon_z(0)$, are accounted for by taking the Laplace transformation of equation (2.29):

$$\begin{bmatrix} s & \omega_{ie}\sin L & 0 & \omega_{ie}\sin L & -s\cos L \\ -\omega_{ie}\sin L & s & -\omega_{ie}\cos L & s & 0 \\ 0 & \omega_{ie}\cos L & s & \omega_{ie}\cos L & s\sin L \\ 0 & -g & 0 & r\,s^2 & r\omega_{ie}\sin 2L\, s \\ g & 0 & 0 & -2r\omega_{ie}\sin L\, s & s^2 r\cos L \end{bmatrix} \begin{bmatrix} \bar{\varepsilon}_N \\ \bar{\varepsilon}_E \\ \bar{\varepsilon}_D \\ \delta\bar{L} \\ \delta\bar{\lambda} \end{bmatrix}$$

$$= \begin{bmatrix} (u)\bar{\omega}_N + \dfrac{\tau_N\,\omega_{ie}\cos L}{s} + \varepsilon_N(0) - \cos L\,\delta\lambda(0) \\ (u)\bar{\omega}_E + \varepsilon_E(0) + \delta L(0) \\ (u)\bar{\omega}_z - \dfrac{\tau_D\,\omega_{ie}\sin L}{s} + \varepsilon_D(0) - \sin L\,\delta\lambda(0) \\ (u)\bar{f}_N - \bar{\xi}g + r[s\,\delta L(0) + \dot{\delta L}(0)] + r\omega_{ie}\sin 2L\,\delta\lambda(0) \\ (u)\bar{f}_E + \bar{\eta}g + r\cos L[s\,\delta\lambda(0) + \dot{\delta\lambda}(0)] - 2r\omega_{ie}\sin L\,\delta L(0) \end{bmatrix} \quad (2.30)$$

where

$s \sim$ Laplace operator

$\tau_N$, $\tau_E$, $\tau_D$ are constant.

Superbar $\sim$ Laplace transformed variable

The signal flow diagram corresponding to equation (2.30) is shown in Figure (2.4).

Note that the characteristic determinant for equation (2.29) is given by:

$$p\,r^2\cos L(p^2 + \omega_{ie}^2)[p^4 + 2\omega_s^2(1 + 2\frac{\omega_{ie}^2}{\omega_s^2}\sin^2 L)\;p^2 + \omega_s^4] \quad (2.31)$$

Thus it is seen that the system modes of oscillation for the stationary case consist of the Earth rate frequency and the Foucault modulated Schuler frequencies.

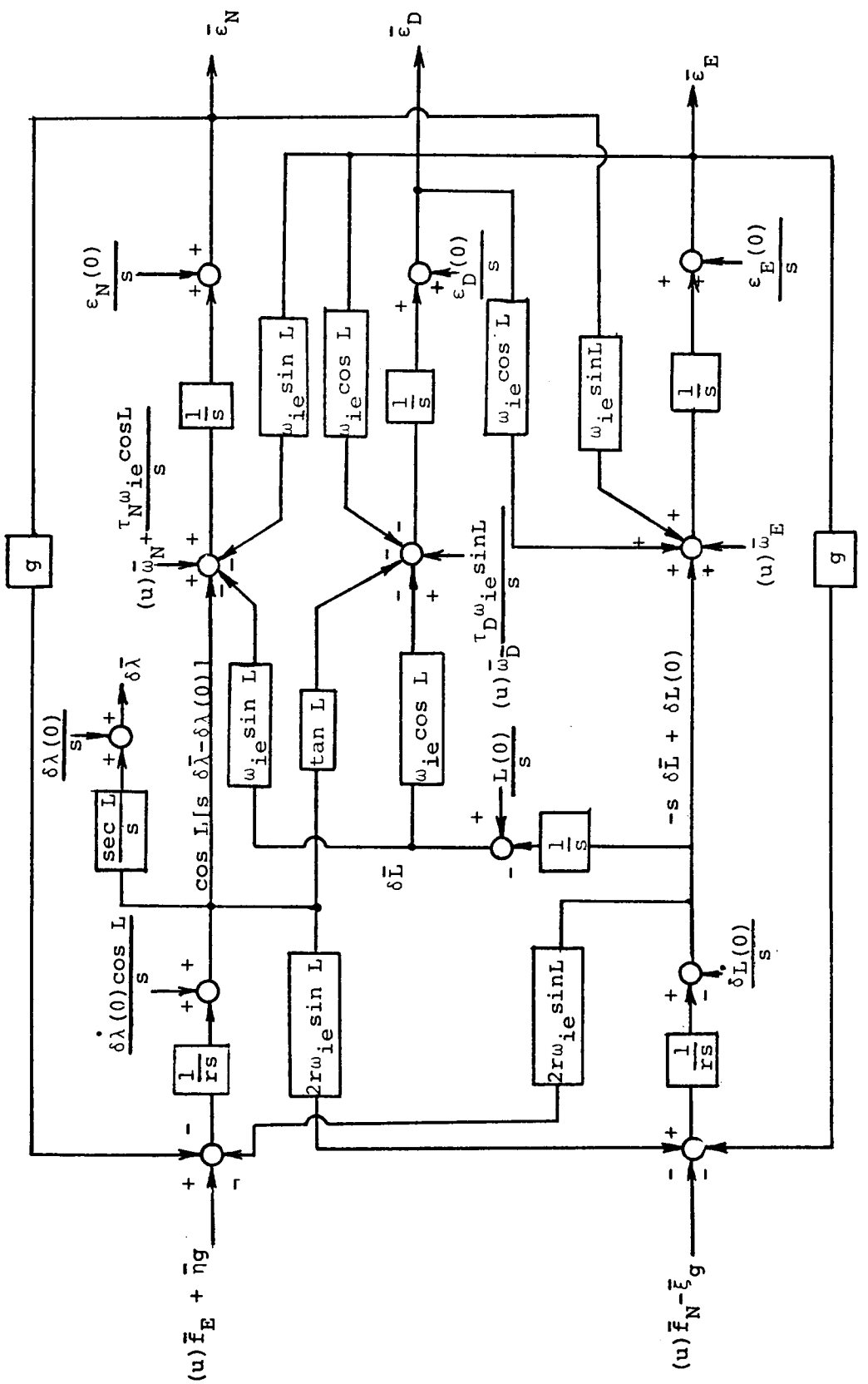


Figure (2.4). Signal Flow for Stationary Local Vertical System

## 2.4.1 Navigation and Level Errors for Constant Gyro Drift

Considering the stationary case and letting constant gyro drift be the sole error source, we have from equation (2.30) that:

$$\begin{bmatrix} s & \omega_{ie}\sin L & 0 & \omega_{ie}\sin L & -s\cos L \\ -\omega_{ie}\sin L & s & -\omega_{ie}\cos L & s & 0 \\ 0 & \omega_{ie}\cos L & s & \omega_{ie}\cos L & s\sin L \\ 0 & -g & 0 & r\,s^2 & r\omega_{ie}\sin 2L\, s \\ g & 0 & 0 & -2r\omega_{ie}\sin L\, s & s^2 r\cos L \end{bmatrix} \begin{bmatrix} \bar{\varepsilon}_N \\ \bar{\varepsilon}_E \\ \bar{\varepsilon}_D \\ \delta\bar{L} \\ \delta\bar{\lambda} \end{bmatrix} = \begin{bmatrix} (u)\,\omega_N/s \\ (u)\,\omega_E/s \\ (u)\,\omega_D/s \\ 0 \\ 0 \end{bmatrix} \tag{2.32}$$

Where $(u)\omega_N$, $(u)\omega_E$, and $(u)\omega_D$ are the constant gyro drift rates associated with the north, east, and azimuth gyros, respectively. Because of the Foucault modulation, equation (2.32) is best solved via use of an analog or digital computer. The results of such a solution at latitude = 45° are shown in Figures (2.5), (2.6), and (2.7). In Fig. (2.7) the level errors were found to be so small (about 0.01 min/meru) as to be buried in the analog computer noise. Note that the effect of the Foucault terms is to modulate the Schuler oscillations at a frequency given by $\omega_{ie}\sin L$ (34 hour period at L = 45°), the vertical projection of earth rate. This modulation arises from the calculation of the accelerometer compensation terms in eqs. (2.8) and (2.9) as will be seen when the equations are rederived, assuming perfect accelerometer compensation. It is seen from these three figures that the Foucault modulation has only a second order effect on the amplitude of the latitude, longitude, and azimuth errors, the predominant mode occurring at the earth rate frequency. On the other hand, for the level errors, $\varepsilon_N$ and $\varepsilon_E$, the Foucault modulation is a first order effect. These results would suggest that for the purposes of design, it would be convenient to neglect the Foucault modulation, obtaining equations which are readily solved and which yield solutions

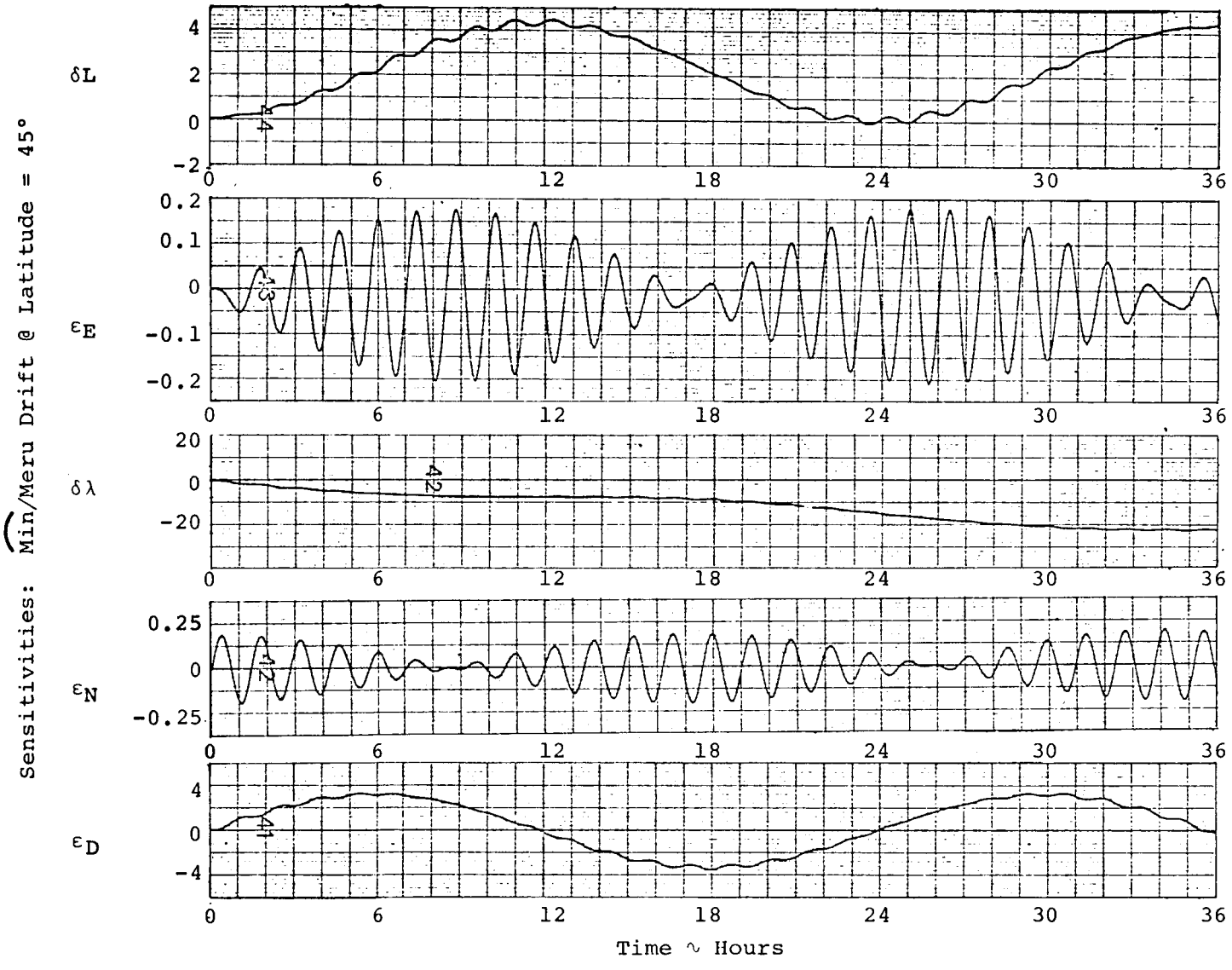


Figure 2.5 ∿ Navigation and Level Errors for Constant North Gyro Drift

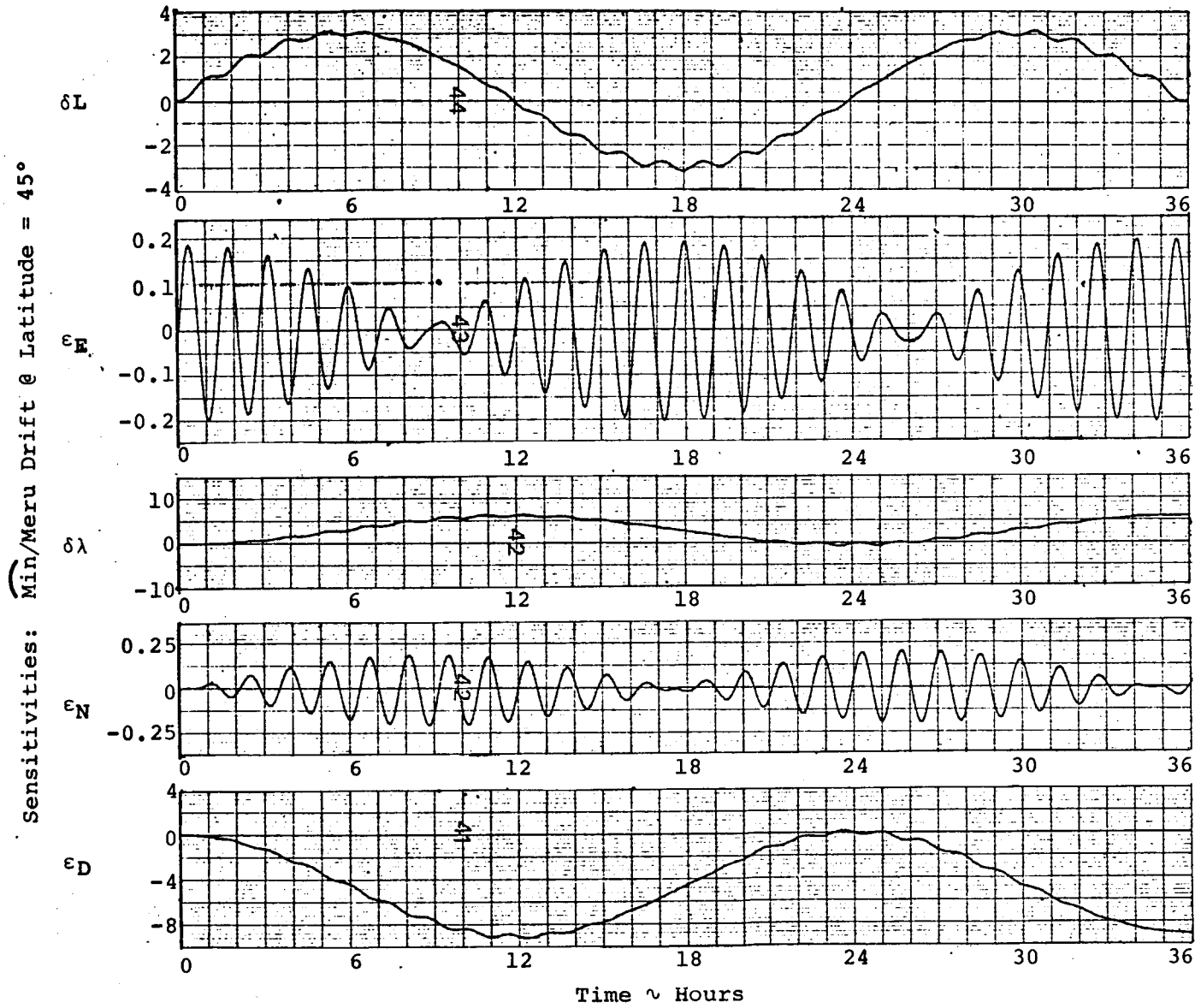


Figure 2.6 ~ Navigation and Level Errors for Constant East Gyro Drift

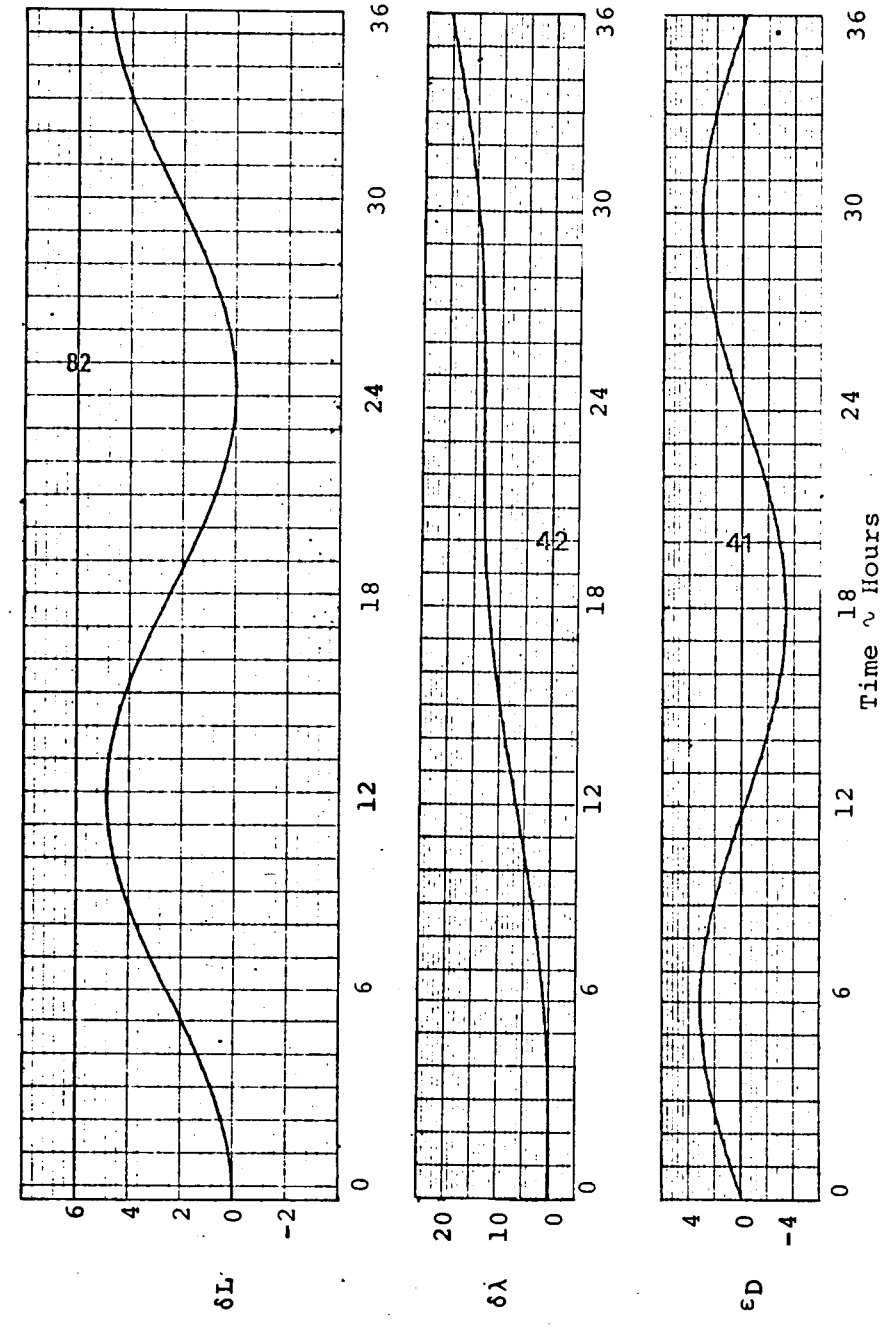


Figure 2.7 ~ Navigation Errors for Constant Azimuth Gyro Drift

which, although differing slightly in frequency content, exhibit approximately the same amplitude information. As indicated by the computer solutions, this approximation will be a very good one for the latitude, longitude, and azimuth errors, but a relatively poor one for the level errors. Fortunately, the level errors are of secondary importance for navigational purposes.

Figures (2.8), (2.9), and (2.10) show the effect of a constant east terrestrial longitude rate ($\dot{\ell} = 3\omega_{ie}$) on the navigation and level error plots for constant gyro drift. At the 45° latitude this would correspond to a vehicle moving in an easterly direction at about 1900 Kt. Comparison with the stationary case curves (Figures (2.5), (2.6), and (2.7)) indicates that the lowest modulation frequency has increased from $\dot{\lambda} = \omega_{ie}$ for the stationary case to $\dot{\lambda} = 4\omega_{ie}$ for the moving case. This phenomenon is easily explained via examination of the characteristic equation for the moving case. It follows from the derivation of eq. (2.30) that the system characteristic determinant for arbitrary constant longitude rate is found by substituting $\dot{\lambda}$ for $\omega_{ie}$ in eq. (2.31):

$$\Delta = pr^2\cos L\,(p^2 + \dot{\lambda}^2)\left[p^4 + 2\omega_s{}^2\left(1 + 2\,\frac{\dot{\lambda}^2}{\omega_s{}^2}\sin^2 L\right)p^2 + \omega_s{}^4\right]$$

The system modes are seen to be the space rate mode and Foucault modulated Schuler frequencies. For this case of $\dot{\lambda} = 4\omega_{ie}$ the space rate period is six hours while the Foucault modulation now occurs with a period of about 8.5 hours instead of the 34 hour period for the stationary case. These six hour and 8.5 hour modes are easily identified in the figures.

Perhaps the most important feature revealed by the comparison is the fact that the latitude and azimuth error sensitivities are reduced from the stationary case by the factor $\omega_{ie}/\dot{\lambda}$, or in this situation for $\dot{\lambda} = 4\omega_{ie}$, by a factor of four. For the cases which exhibit a longitude error which grows with time, namely the responses to $(u)\omega_N$ and $(u)\omega_D$, the vehicle motion appears to have little effect on the error growth. On the other

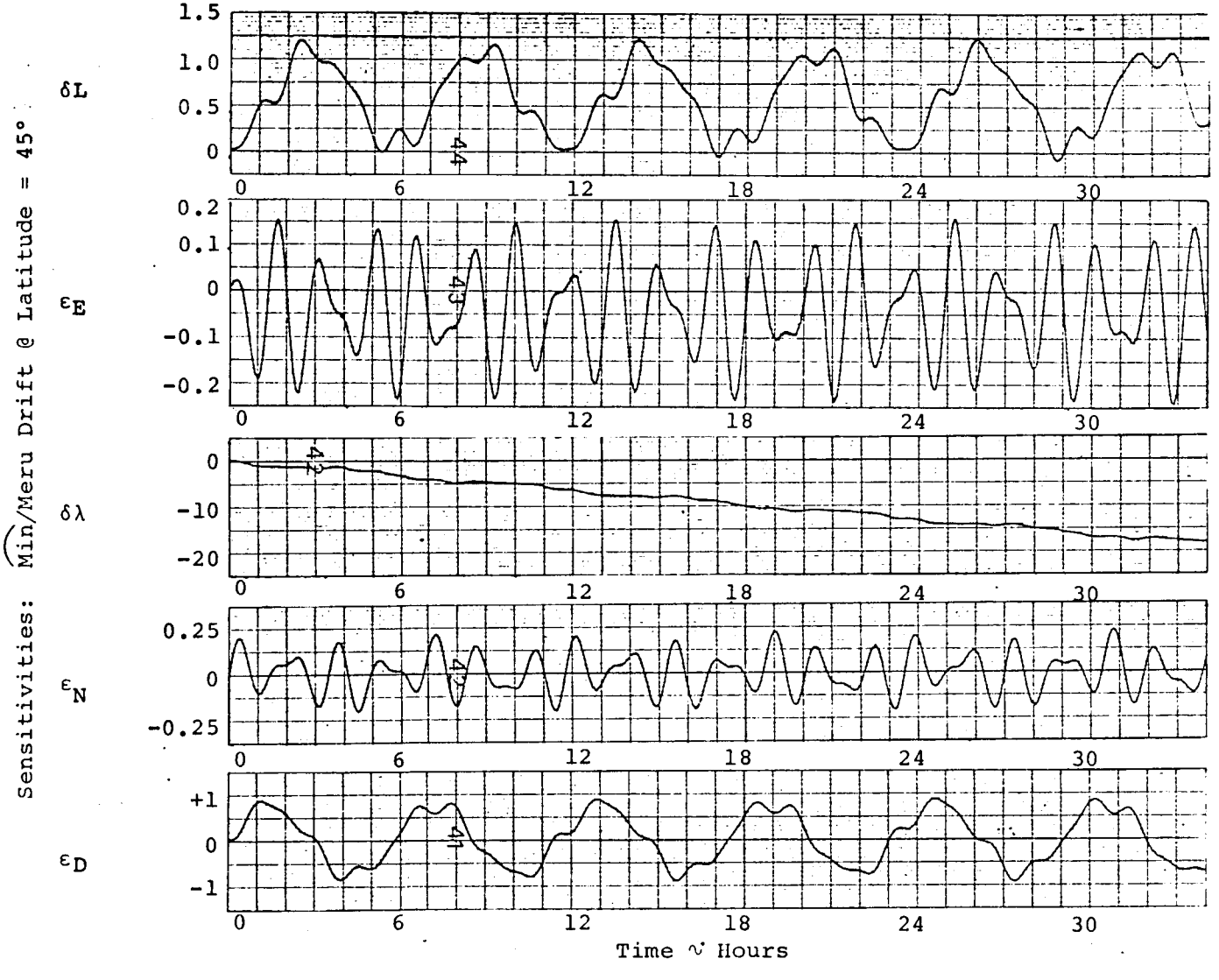


Figure 2.8 ∿ Navigation and Level Errors for Constant North and Gyro Drift at East Terrestrial Velocity of 1900 Kt.

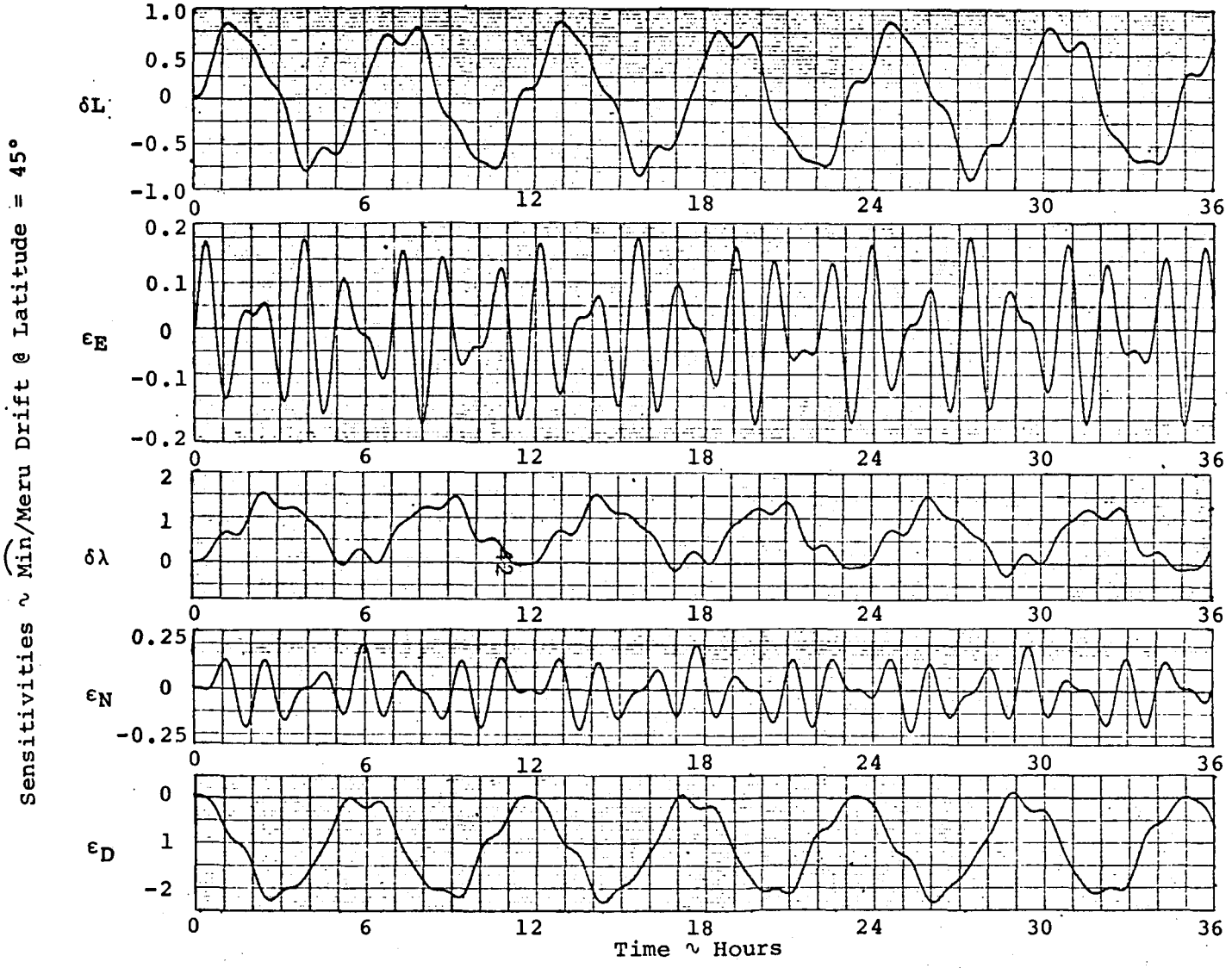


Figure 2.9 ~ Navigation and Level Errors for Constant East Gyro Drift at East Terrestrial Velocity of 1900 Kt.

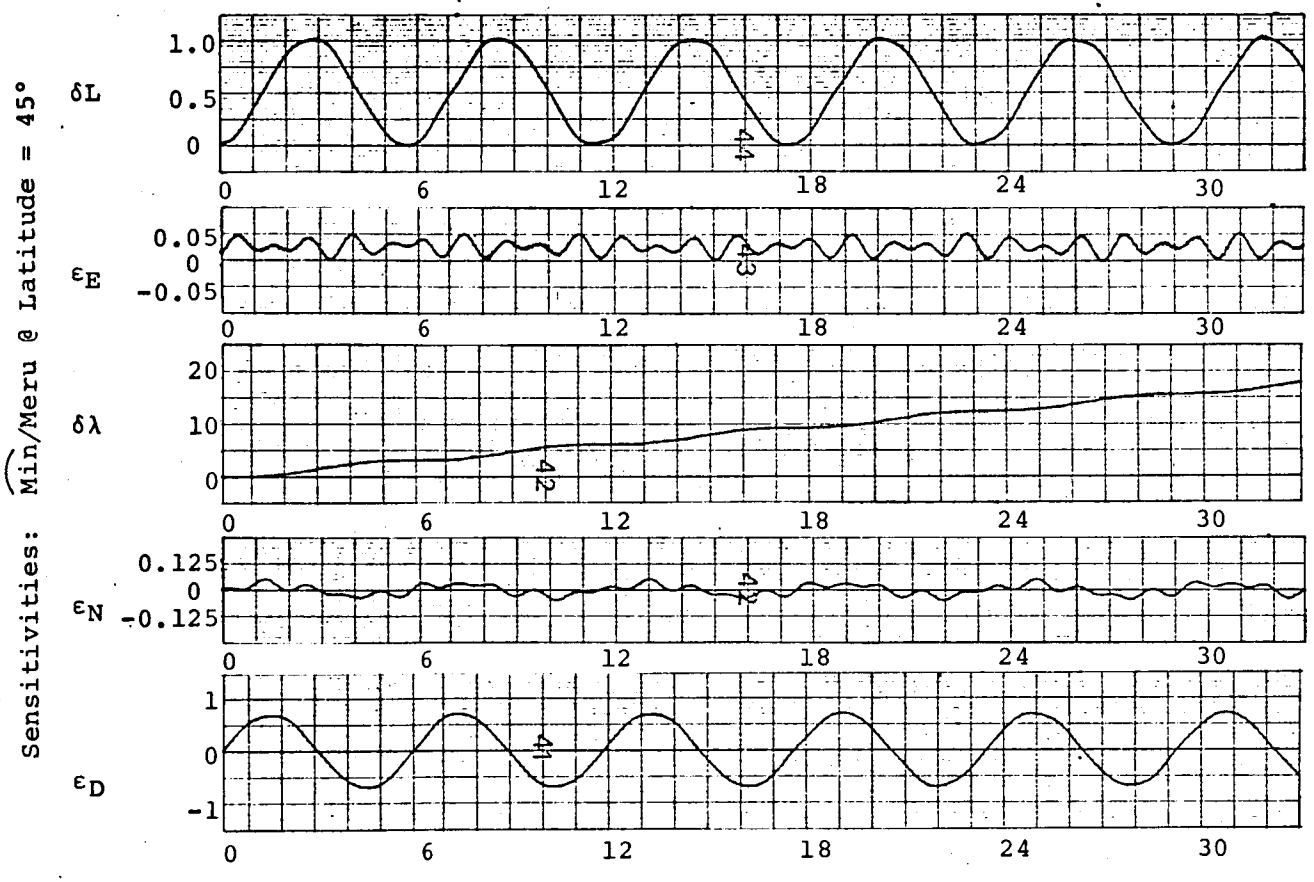


Figure 2.10 ∿ Navigation and Level Errors for Constant Azimuth Gyro Drift at East Terrestrial Velocity of 1900 Kt.

hand, the sensitivity $\delta\lambda/(u)\omega_E$, which is bounded for the stationary case, is reduced by the factor $\omega_{ie}/\dot{\lambda}$. The level error sensitivities in response to level gyro drift are seen to remain unchanged while the level error response to azimuth gyro drift is seen to emerge from the computer noise. A digital computer solution has revealed that these error sensitivities, $\varepsilon_E/(u)\omega_D$ and $\varepsilon_N/(u)\omega_D$, have in fact increased by the factor $\dot{\lambda}/\omega_{ie}$. Examination of the signal flow diagram, Figure 2.4, reveals that the coupling sensitivity between the azimuth and east level loop is increased by the required factor of $\dot{\lambda}/\omega_{ie}$.

An interesting limiting case arises when the vehicle is flying west with $\dot{\ell} = -\omega_{ie}$. This case is readily analyzed by setting $\omega_{ie}$ to zero in Figure 2.4, thereby eliminating the Foucault and space rate coupling. The level error sensitivities remain unchanged sans the Foucault modulation, but the latitude, longitude, and azimuth errors grow in proportion to the product of the drift rate and time. Specifically, for times greater than a Schuler period,

$$\delta L \approx (u)\omega_E t$$

$$\delta\lambda \approx -(u)\omega_N t \tan L$$

$$\varepsilon_D \approx (u)\omega_N t \tan L + (u)\omega_D t$$

Thus a maximum navigational error sensitivity of about 1 $\widehat{\text{min}}$/hr/meru drift represents an upper bound on the sensitivity to gyro drift regardless of vehicle motion.

A similar uncoupling effect occurs for operation near the equator for arbitrary celestial longitude rate. If we let the latitude approach zero degrees in Figure 2.4, it is readily seen that the terms responsible for the Foucault modulation, the "$2r\omega_{ie}$ sin L" terms, disappear and in addition the north level loop becomes completely uncoupled from the latitude, azimuth, and east level loops.

Since it has been shown that the Foucault modulation of the Schuler oscillations have only a second order effect on the navigational errors, it will be useful to obtain analytical expressions for the system response to gyro drift which are not complicated by the Foucault modulation. It follows from the development leading to equations (2.18) and (2.19) that if the accelerometer compensation is performed without error, the appropriate equations corresponding to equations (2.18) and (2.19) for the stationary case are given by:

$$r\,\delta\ddot{L} - g\,\varepsilon_E = -\xi g + (u) f_N \tag{2.33}$$

$$r\cos L\,\delta\ddot{\lambda} + g\,\varepsilon_N = \eta g + (u) f_E \tag{2.34}$$

Since simultaneous solution of equations (2.25), (2.26), (2.27), (2.33), and (2.34) is desired, we have the Laplace transformed matrix equation:

$$\begin{bmatrix} s & \omega_{ie}\sin L & 0 & \omega_{ie}\sin L & -s\cos L \\ -\omega_{ie}\sin L & s & -\omega_{ie}\cos L & s & 0 \\ 0 & \omega_{ie}\cos L & s & \omega_{ie}\cos L & s\sin L \\ 0 & -g & 0 & r s^2 & 0 \\ g & 0 & 0 & 0 & s^2 r\cos L \end{bmatrix} \begin{bmatrix} \bar{\varepsilon}_N \\ \bar{\varepsilon}_E \\ \bar{\varepsilon}_D \\ \delta\bar{L} \\ \delta\bar{\lambda} \end{bmatrix} =$$

$$\begin{bmatrix} (u)\bar{\omega}_N + \dfrac{\tau_N \omega_{ie}\ \cos L}{s} + \varepsilon_N(0) - \cos L\ \delta\lambda(0) \\ (u)\bar{\omega}_E + \varepsilon_E(0) + \delta L(0) \\ (u)\bar{\omega}_D - \dfrac{\tau_D \omega_{ie}\ \sin L}{s} + \varepsilon_D(0) - \sin L\ \delta\lambda(0) \\ (u)\bar{f}_N - \bar{\xi} g + r[s\ \delta L(0) + \dot{\delta L}(0)] \\ (u)\bar{f}_E + \bar{\eta} g + r \cos L\ [s\ \delta\lambda(0) + \dot{\lambda}(0)] \end{bmatrix} \qquad (2.35)$$

Eq. (2.35) represents the Laplace transformed error equation for a stationary local vertical inertial navigation system in which the accelerometer compensation is done withour error. If constant gyro drift is the sole error source, equation (2.35) reduces to:

$$\begin{bmatrix} s & \omega_{ie}\sin L & 0 & \omega_{ie}\sin L & -s\cos L \\ -\omega_{ie}\sin L & s & -\omega_{ie}\cos L & s & 0 \\ 0 & \omega_{ie}\cos L & s & \omega_{ie}\cos L & s\sin L \\ 0 & -g & 0 & r s^2 & 0 \\ g & 0 & 0 & 0 & s^2 r \cos L \end{bmatrix} \begin{bmatrix} \bar{\varepsilon}_N \\ \bar{\varepsilon}_E \\ \bar{\varepsilon}_D \\ \delta\bar{L} \\ \delta\bar{\lambda} \end{bmatrix} = \begin{bmatrix} \dfrac{(u)\omega_N}{s} \\ \dfrac{(u)\omega_E}{s} \\ \dfrac{(u)\omega_D}{s} \\ 0 \\ 0 \end{bmatrix} \qquad (2.36)$$

The system characteristic equation is given by the determinant of the above 5 x 5 matrix:

$$\Delta = r^2 \cos L\ s(s^2 + \omega_s^2)^2(s^2 + \omega_{ie}^2) \qquad (2.37)$$

Solution of Eq. (2.36) yields:

$$\bar{\varepsilon}_N = \frac{s^2 + \omega_{ie}^2 \cos^2 L}{(s^2 + \omega_s^2)(s^2 + \omega_{ie}^2)} (u)\omega_N - \frac{\omega_{ie} \sin L\, s}{(s^2 + \omega_s^2)(s^2 + \omega_{ie}^2)} (u)\omega_E$$

$$- \frac{\omega_{ie}^2 \sin L \cos L}{(s^2 + \omega_s^2)(s^2 + \omega_{ie}^2)} (u)\omega_D \qquad (2.38)$$

$$\bar{\varepsilon}_E = \frac{\omega_{ie} \sin L\, s}{(s^2 + \omega_s^2)(s^2 + \omega_{ie}^2)} (u)\omega_N + \frac{s^2}{(s^2 + \omega_s^2)(s^2 + \omega_{ie}^2)} (u)\omega_E$$

$$+ \frac{\omega_{ie} \cos L\, s}{(s^2 + \omega_s^2)(s^2 + \omega_{ie}^2)} (u)\omega_D \qquad (2.39)$$

$$\bar{\varepsilon}_D = \frac{\tan L(\omega_s^2 - \omega_{ie}^2 \cos^2 L)}{(s^2 + \omega_s^2)(s^2 + \omega_{ie}^2)} (u)\omega_N - \frac{\omega_{ie} \cos L(s^2 + \omega_s^2 \sec^2 L)}{s(s^2 + \omega_s^2)(s^2 + \omega_{ie}^2)} (u)\omega_E$$

$$+ \frac{(s^2 + \omega_s^2 + \omega_{ie}^2 \sin^2 L)}{(s^2 + \omega_{ie}^2)(s^2 + \omega_s^2)} (u)\omega_D \qquad (2.40)$$

$$\delta\bar{L} = \frac{\omega_s^2 \omega_{ie} \sin L}{s(s^2 + \omega_s^2)(s^2 + \omega_{ie}^2)} (u)\omega_N + \frac{\omega_s^2}{(s^2 + \omega_s^2)(s^2 + \omega_{ie}^2)} (u)\omega_E$$

$$+ \frac{\omega_{ie} \omega_s^2 \cos L}{s(s^2 + \omega_s^2)(s^2 + \omega_{ie}^2)} (u)\omega_D \qquad (2.41)$$

$$\delta\bar{\lambda} = -\frac{\omega_s^2 \sec L\,(s^2 + \omega_{ie}^2 \cos^2 L)}{s^2(s^2+\omega_s^2)(s^2+\omega_{ie}^2)}(u)\omega_N + \frac{\omega_s^2\,\omega_{ie}\tan L}{s(s^2+\omega_s^2)(s^2+\omega_{ie}^2)}(u)\omega_E$$

$$+ \frac{\omega_s^2\,\omega_{ie}^2 \sin L}{s(s^2+\omega_{ie}^2)(s^2+\omega_s^2)}(u)\omega_D \qquad (2.42)$$

The inverse Laplace transformation of the above equation is given by:

$$\varepsilon_N \simeq \frac{1}{\omega_s}\sin\omega_s t\,(u)\omega_N - \frac{\omega_{ie}\sin L}{\omega_s^2}(\cos\omega_{ie}t - \cos\omega_s t)\,(u)\omega_E$$

$$- \frac{\omega_{ie}}{\omega_s^2}\sin L\cos L\sin\omega_{ie}t\,(u)\omega_D \qquad (2.43)$$

$$\varepsilon_E \simeq \frac{\omega_{ie}\sin L}{\omega_s^2}(\cos\omega_{ie}t - \cos\omega_s t)(u)\omega_N + \frac{1}{\omega_s}\sin\omega_s t(u)\omega_E$$

$$+ \frac{\omega_{ie}\cos L}{\omega_s^2}(\cos\omega_{ie}t - \cos\omega_s t)\,(u)\omega_D \qquad (2.44)$$

$$\varepsilon_D \simeq \frac{\tan L}{\omega_{ie}}\sin\omega_{ie}t\,(u)\omega_N - \frac{\sec L}{\omega_{ie}}(1-\cos\omega_{ie}t)\,(u)\omega_E$$

$$+ \frac{1}{\omega_{ie}}\sin\omega_{ie}t\,(u)\omega_D \qquad (2.45)$$

$$\delta L \simeq \frac{1}{\omega_{ie}}(1-\cos\omega_{ie}t)\,[\sin L\,(u)\omega_N + \cos L\,(u)\omega_D]$$

$$+ \frac{1}{\omega_{ie}}\sin\omega_{ie}t\,(u)\omega_E \qquad (2.46)$$

$$\delta\lambda \simeq -\frac{1}{\omega_{ie}}\left(\omega_{ie}t\cos L + \frac{\sin^2 L}{\cos L}\sin\omega_{ie}t\right)(u)\omega_N$$

$$+\frac{\tan L}{\omega_{ie}}\left(1-\cos\omega_{ie}t\right)(u)\omega_E$$

$$+\frac{\sin L}{\omega_{ie}}\left(\omega_{ie}t-\sin\omega_{ie}t\right)(u)\omega_D \qquad (2.47)$$

Where it was noted that $\omega_s >> \omega_{ie}$, allowing us to neglect certain terms whose coeficients were of the form $\frac{\omega_{ie}}{\omega_s}$ and $\frac{\omega_{ie}^2}{\omega_s^2}$.

If equations (2.46) and (2.47) are compared with the computer generated solutions of Figure (2.5), it is seen that the simplified expressions for latitude and longitude do not contain the small amplitude Schuler-Foucault terms. However, the dominating earth rate mode is accurately specified by the simplified equations. Thus equation (2.35) will be taken as a representative error model for the stationary local vertical inertial navigator in response to constant gyro drift.

Note that one can, by careful examination of the signal flow diagram in Figure (2.4), predict the response to the various error sources by inspection. For instance, if we take the case of $\varepsilon_N$(eq. 2.43), one expects to see that

$$\frac{\partial\varepsilon_N}{\partial(u)\omega_N} = \frac{1}{\omega_s}\sin\omega_s t\,(u)\omega_N$$

since the Earth rate cross coupling from the north loop to the east loop ($\omega_{ie}$ sin L $\bar{\varepsilon}_N$) is attenuated by the east level loop before being coupling back to the north loop ($\omega_{ie}$ sin L $\bar{\varepsilon}_E$). Thus the response to $\varepsilon_N$ to $(u)\omega_N$ is seen by examination of the response of the following system:

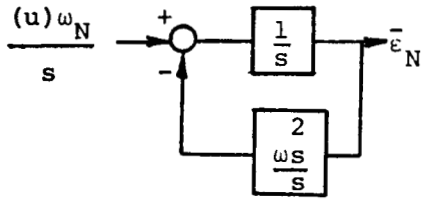


Thus $\bar{\varepsilon}_N = \frac{(u)\omega_N}{s^2+\omega_s^2} \rightarrow \varepsilon_N = \frac{1}{\omega_s} \sin \omega_s t$

Root sum squared plots of eqs. (2.43), (2.44), (2.45), (2.46), and (2.47) are shown in Figure 2.11 for the case of equal gyro drift for each gyro:

$$(u)\omega_N = (u)\omega_E = (u)\omega_D = (u)\omega$$

The analytic expressions used in Figure 2.11 are given by:

$$\varepsilon_{N_{RSS}} = \varepsilon_{E_{RSS}} = \frac{(u)\omega}{\omega_s} \left|\sin\omega_s t\right| \qquad (2.48)$$

$$\delta L_{RSS} = \frac{\varepsilon_{D_{RSS}}}{\sec L} = \sqrt{2}\, \frac{(u)\omega}{\omega_{ie}} (1 - \cos \omega_{ie} t)^{1/2} \qquad (2.49)$$

$$\delta\lambda_{RSS} = \frac{(u)\omega}{\omega_{ie}} [\omega_{ie}^2 t^2 + 2 (1-\cos \omega_{ie} t)]^{1/2}, \text{ at } L = 45° \qquad (2.50)$$

Note that the level, azimuth, and latitude errors are bounded, but that the longitude error increases withour bound with a rate approximately given by the gyro drift uncertainty, $(u)\omega$.

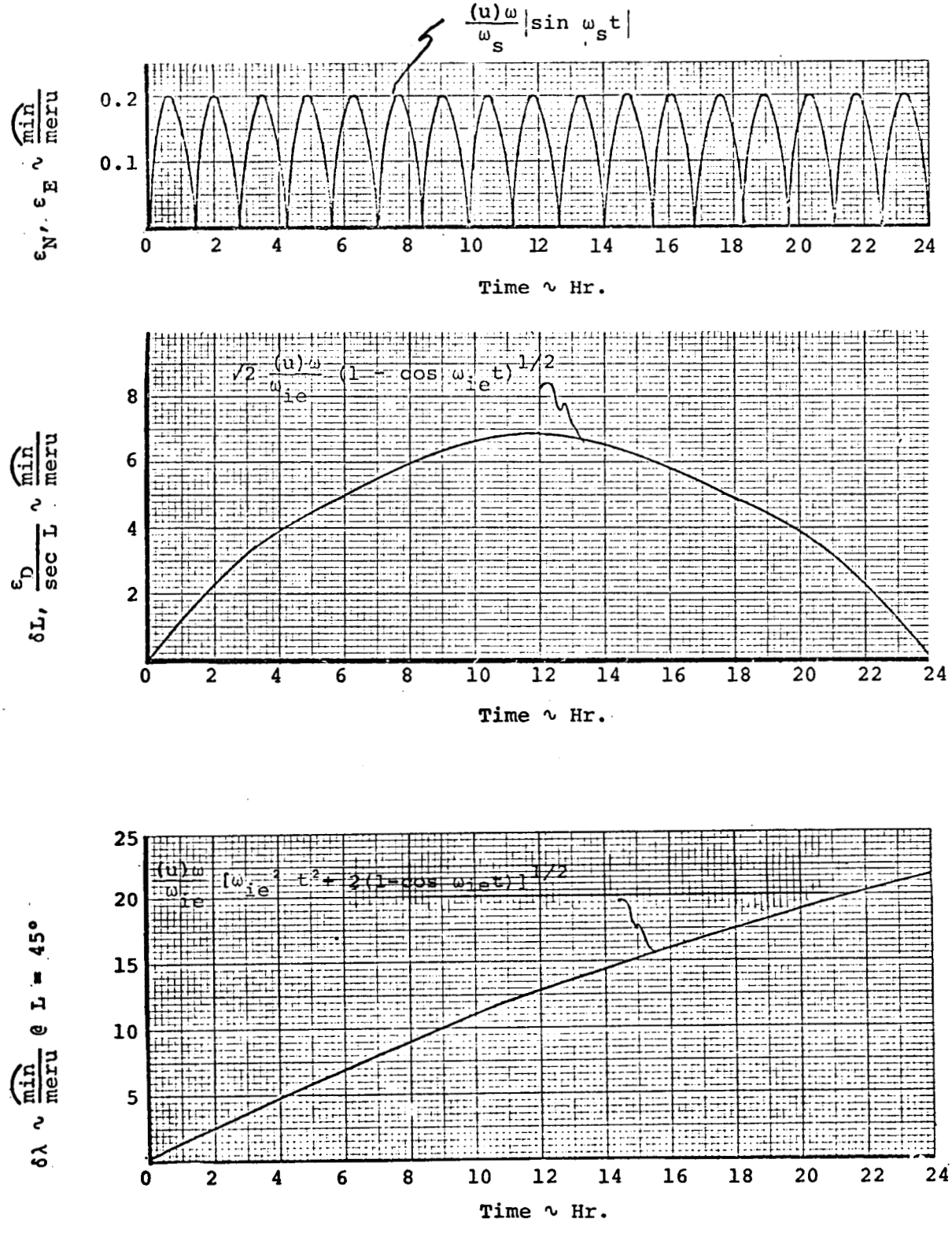


Figure 2.11∿Local Vertical I.N.S. Navigation Errors (Perfect Coriolis Compensation) ∿ Root Sum Squared

2.4.2 Navigation and Level Errors for Accelerometer Bias

If accelerometer bias is the sole error source, we have from equation (2.30) that:

$$\begin{bmatrix} s & \omega_{ie}\sin L & 0 & \omega_{ie}\sin L & -s\cos L \\ -\omega_{ie}\sin L & s & -\omega_{ie}\cos L & s & 0 \\ 0 & \omega_{ie}\cos L & s & \omega_{ie}\cos L & s\sin L \\ 0 & -g & 0 & r\,s^2 & r\omega_{ie}\sin 2L\; s \\ g & 0 & 0 & -2r\omega_{ie}\sin L\; s & s^2 r\cos L \end{bmatrix} \begin{bmatrix} \bar{\varepsilon}_N \\ \bar{\varepsilon}_E \\ \bar{\varepsilon}_D \\ \bar{\delta}L \\ \delta\bar{\lambda} \end{bmatrix} = \begin{bmatrix} 0 \\ 0 \\ 0 \\ \dfrac{(u)f_N}{s} \\ \dfrac{(u)f_E}{s} \end{bmatrix} \quad (2.51$$

Where $(u)f_N$ and $(u)f_E$ are the constant north and east accelerometer biasses, respectively. Figures 2.12 and 2.13 show the results of a computer solution of eq. (2.51). Note that the Schuler mode predominates since the accelerometer bias directly excites the relatively "high gain" level loops. The Schuler oscillations are modulated at the Foucault mode frequency of 1 cycle/36 hours. The maximum sensitivity of latitude error to accelerometer bias is seen to be in the range of 7 $\widehat{\text{min}}$/milli g bias. Similarly, the longitude sensitivity has a maximum value of about 9 $\widehat{\text{min}}$/milli g bias.

If the effect of the accelerometer compensation is neglected, as was done in obtaining analytic solutions for gyro drift (eq. 2.36), the following solutions are obtained:

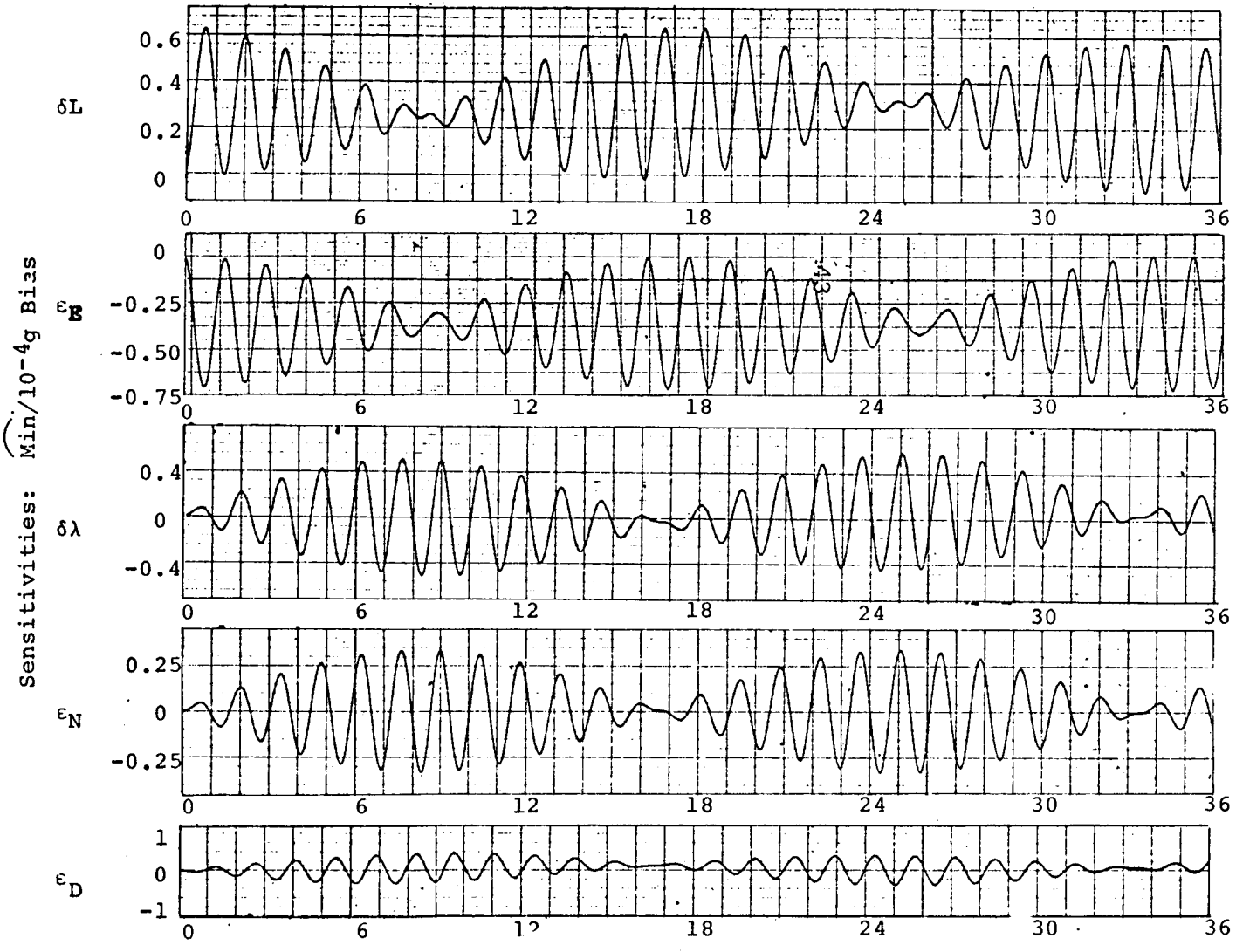


Figure 2.12 ∿ Navigation and Level Errors for North Accelerometer Bias

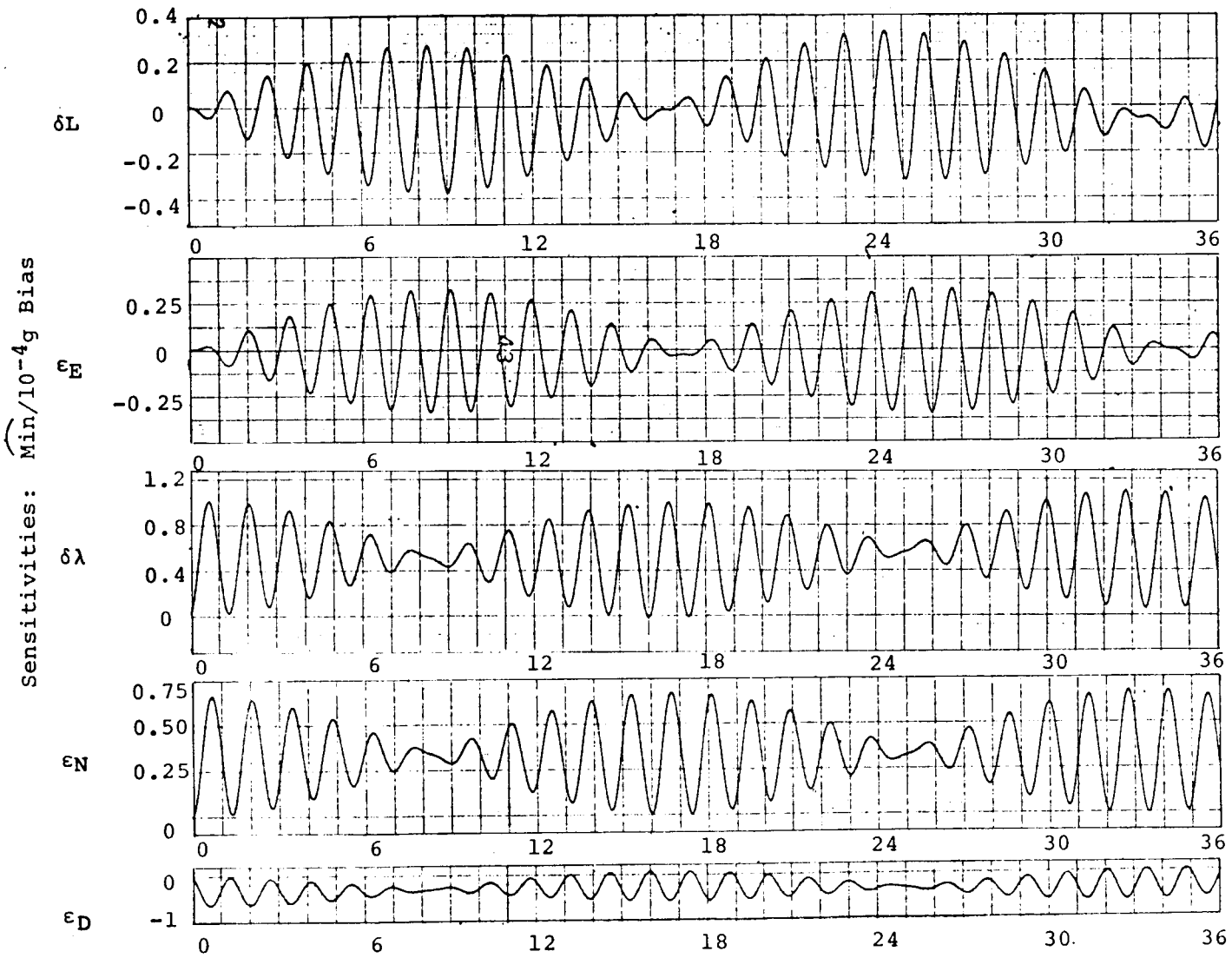


Figure 2.13 ∿ Navigation and Level Errors for East Accelerometer Bias

$$\varepsilon_N = (1 - \cos\omega_s t)\ \frac{(u)f_E}{g} \tag{2.52}$$

$$\varepsilon_E = -(1 - \cos\omega_s t)\ \frac{(u)f_N}{g} \tag{2.53}$$

$$\varepsilon_D = -\tan L\ (1 - \cos\omega_s t)\ \frac{(u)f_E}{g} \tag{2.54}$$

$$\delta L = (1 - \cos\omega_s t)\ \frac{(u)f_N}{g} \tag{2.55}$$

$$\delta\lambda = \sec L\ (1 - \cos\omega_s t)\ \frac{(u)f_E}{g} \tag{2.56}$$

Note that these solutions neglect the effects of the Foucault modulations, first order effects. In addition, the cross coupling effects shown in Figures 2.12 and 2.13 are completely neglected. If, however, the above analytic solutions are compared with the computer generated solutions, it is concluded that neglecting the accelerometer compensation yeilds results which are quite accurate for periods of time up to about one Schuler period (84 minutes). Thus if one is interested in modeling a local vertical inertial navigation system for short periods of time, which would be the case for an aided inertial system, the simplified model obtained by neglecting the accelerometer compensation would be perfectly adequate.

Figure 2.14 shows the effect of a 1900 Kt. east terrestrial velocity on the error response to accelerometer bias. The Foucault modulating frequency is increased by a factor of $\frac{\dot{\lambda}}{\omega_{ie}} = 4$ and the error sensitivities are seen to remain unchanged. In the limiting case mentioned previously when $\dot{\ell} = -\omega_{ie}$, the Foucault modulation disappears completely leaving a pure Schuler oscillation. In addition, the cross coupling is eliminated and the response is accurately described by equations (2.52) through (2.56).

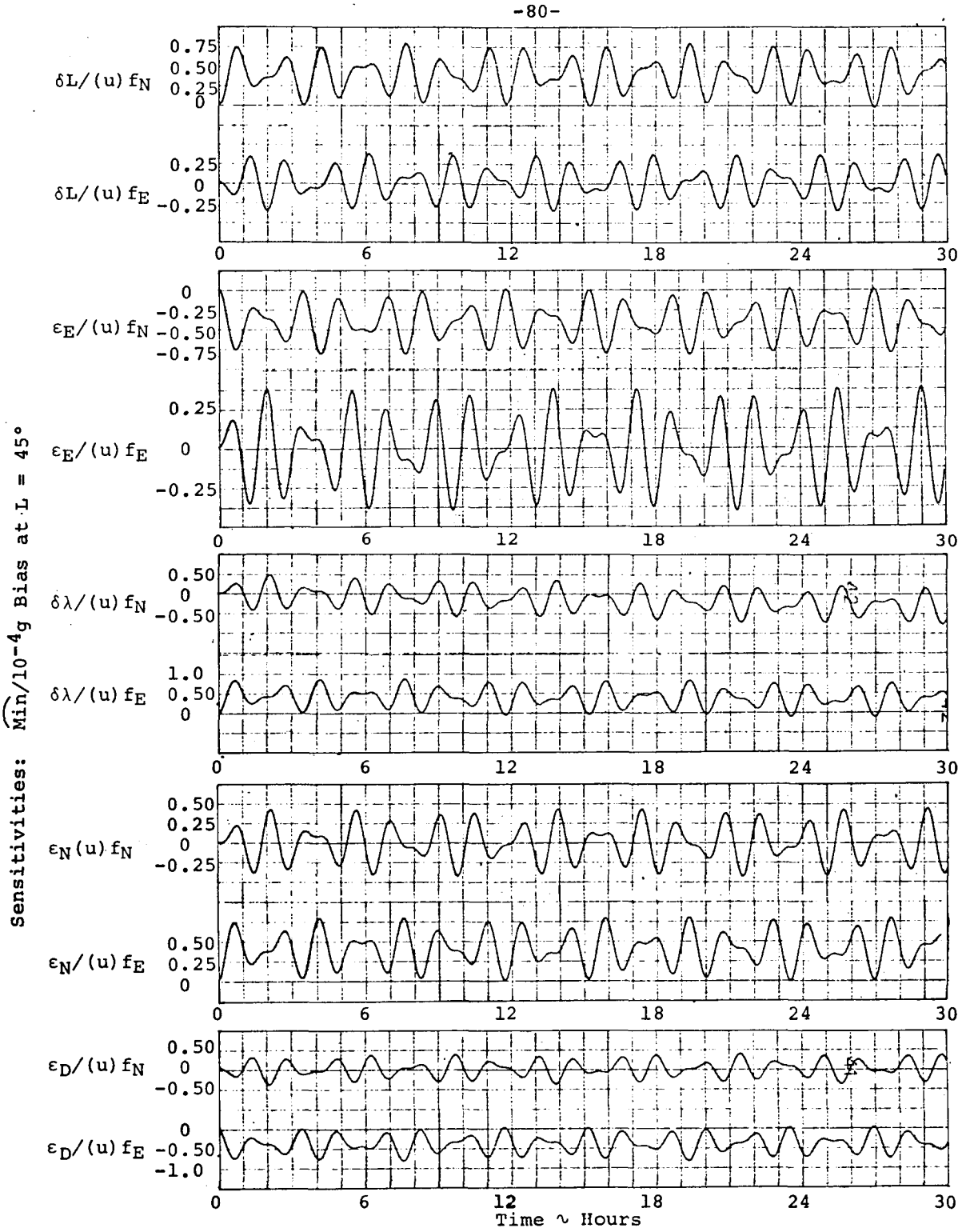


Figure 2.14 ∿ Navigation and Level Errors for Accelerometer Bias at East Terrestrial Velocity of 1900 Kt.

2.4.3 Latitude and Longitude Rate Errors

Figure 2.15 shows computer derived plots of latitude and longitude rate errors for the case of constant gyro drift and accelerometer bias. These errors are easily related to the north and east velocity errors since from Pg.44 , for $\dot{\lambda} = \omega_{ie}$

$$\delta v_N \cong r\, \delta\dot{L} \tag{2.57}$$

$$\delta v_E \cong r\, \delta\dot{\lambda} \cos L \tag{2.58}$$

where

$\delta v_N \sim$ north velocity error
$\delta v_E \sim$ east velocity error

It is seen, therefore, that the north and east peak velocity sensitivity to level gyro drift is about 1.35 $\frac{\text{n.m.}}{\text{hr}}$/meru drift (1 n.m./hr $\cong$ 1.7 ft/sec), while the sensitivity to azimuth gyro drift is about 0.75 $\frac{\text{n.m.}}{\text{hr}}$/meru drift. Peak velocity errors due to accelerometer bias are seen to be about 1.25 $\frac{\text{n.m.}}{\text{hr}}/10^{-4}$g bias. Note the particularly interesting effect of the three system modes of oscillation in response to level gyro dirft.

Latitude and longitude rate error plots are shown in Figure 2.16 for the case of a constant east terrestrial velocity of 1900 Kt. Comparison of Figures 2.14 and 2.15 reveals that the rate error magnitudes are unaffected by the vehicle motion, a result which is not too surprising since the level error magnitudes were previously shown to be virtually unaffected by vehicle motion. Note that for the case of this rather high terrestrial longitude rate, Eq. (2.58) does not yield the total east velocity error. In particular, for $\dot{\lambda} \neq \omega_{ie}$, the appropriate expression for the east velocity error is given by:

$$\delta v_E = r\, \delta\dot{\lambda} \cos L - r\, \dot{\ell}\, \delta L \sin L$$

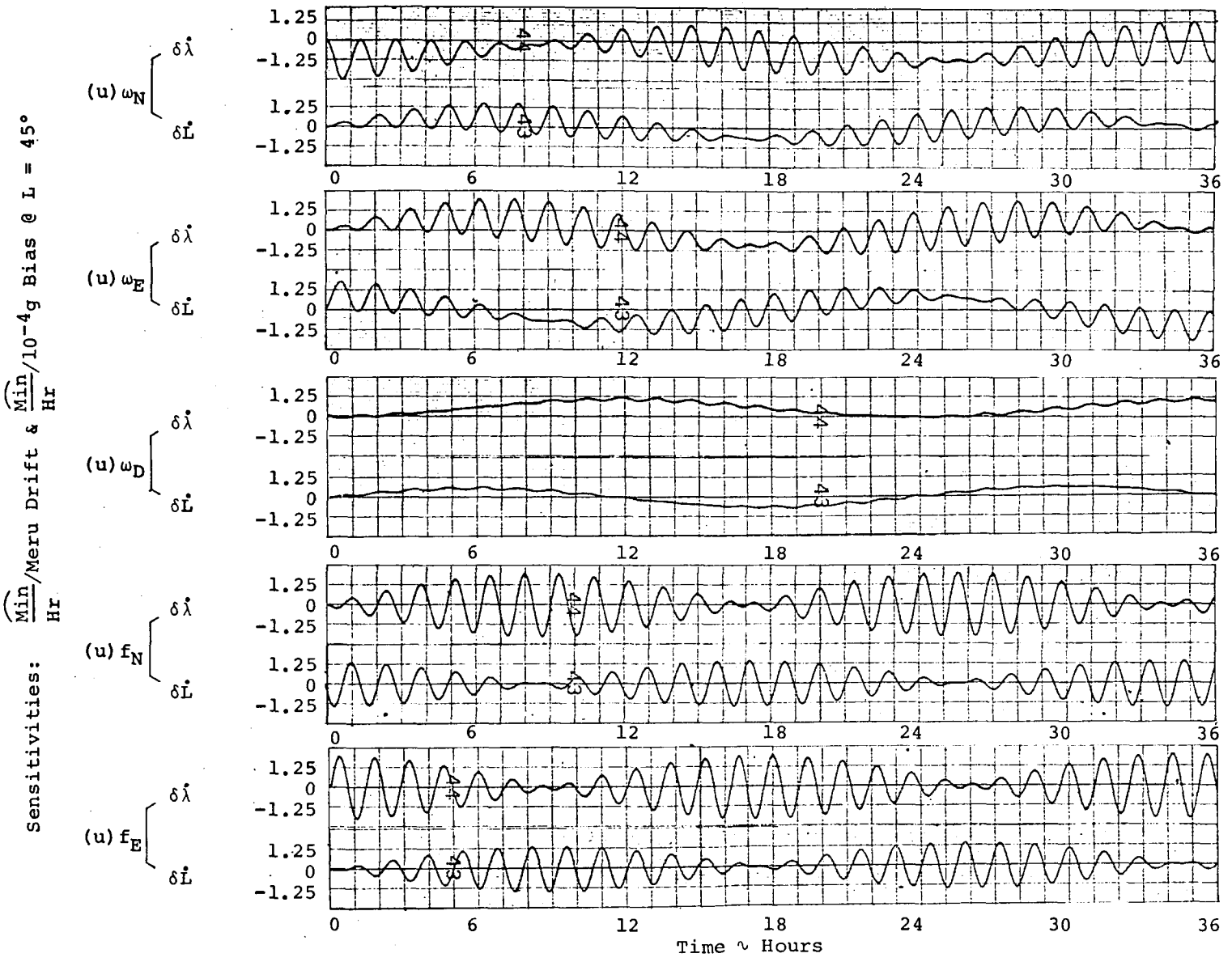


Figure 2.15 ∿ Latitude and Longitude Rate Errors

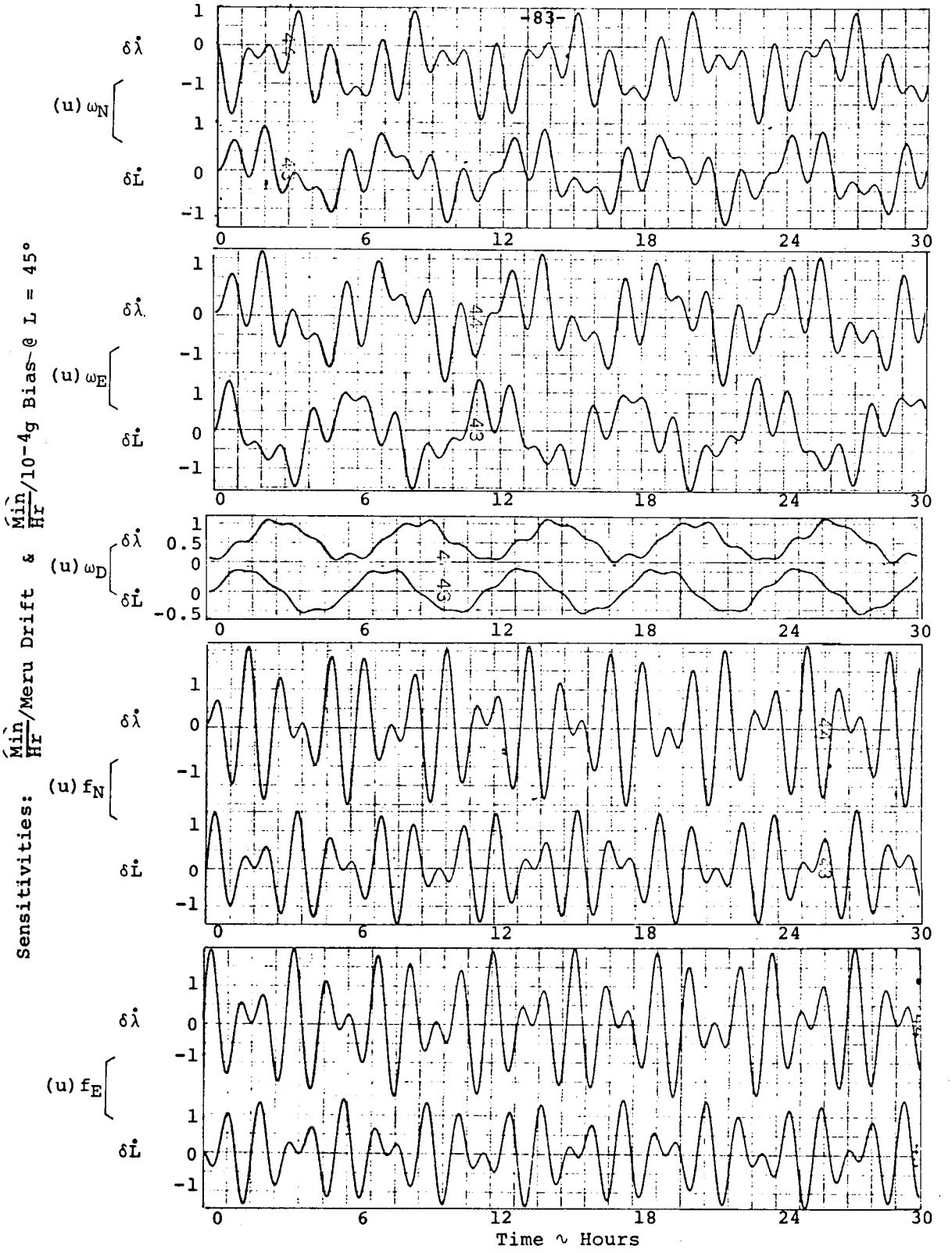


Figure 2.16 ∿ Latitude and Longitude Rate Errors at East Terrestrial Velocity of 1900 Kt.

2.4.4 Initial Condition Errors

Figures 2.17 through 2.21 show computer solutions of the error response to initial north level, east level, latitude, latitude rate, and longitude rate errors, respectively. Please note that the response is shown for negative initial condition errors. The response to initial longitude error is not shown because, as seen in Figure 2.4, longitude is uncoupled from the other computation loops. Thus the system response to initial longitude error is simply:

$$\delta\lambda = \int_o^t \delta\lambda(0)\, dt \qquad (2.59)$$

A constant initial condition error therefore results in a longitude error growth rate of 1 $\widehat{\text{min}}/\text{hr}/\widehat{\text{min}}$ uncertainty. The response to initial azimuth error is also not shown since it is seen from Figure 2.4 that the response is identical to that due to constant east gyro drift. Thus Figure 2.6 and the $(u)\omega_E$ response of Figure 2.15 can be used with the sensitivity given by:

$$\frac{\varepsilon_D(0)\ \omega_{ie}\ \cos L}{(u)\omega_E} \cong \frac{\cos L}{3.44} \cong 0.206\ \frac{\widehat{\text{min}}/\widehat{\text{min}}\ \varepsilon_D(0)}{\widehat{\text{min}}/\text{meru}\ (u)\omega_E}$$

for the case of Figure 2.6, and the same numerical sensitivity with the appropriate units for the case of Figure 2.15.

For the purposes of design, it is convenient to obtain analytic expressions for the response to initial condition errors. As before, this solution is most conveniently effected by solving the matrix equation 2.30 with the Foucault modes omitted. The results of such a solution for arbitrary finite constant celestial longitude rate, $\dot{\lambda}$ = constant, is given by the following equation:

$$\underline{x} = \underline{A}\,\underline{x}(0) \qquad (2.60)$$

where

$$\underline{x} = \{\varepsilon_N,\ \varepsilon_E,\ \varepsilon_D,\ \delta L,\ \delta\lambda,\ \delta\dot{L},\ \delta\dot{\lambda}\},$$

$$\underline{x}(0) = \{\varepsilon_N(0),\ \varepsilon_E(0),\ \varepsilon_D(0),\ \delta L(0),\ \delta\lambda(0),\ \delta\dot{L}(0),\ \delta\dot{\lambda}(0)\},$$

and

$$\underline{A} = \begin{bmatrix}
\cos\omega_s t & -\frac{\dot{\lambda}}{\omega_s}\sin L(\sin\omega_s t - \frac{\dot{\lambda}}{\omega_s}\sin\dot{\lambda}t) & \frac{1}{2}\frac{\dot{\lambda}^2}{\omega_s^2}\sin 2L(\cos\omega_s t - \cos\dot{\lambda}t) & -\frac{\dot{\lambda}}{\omega_s}\sin L(\sin\omega_s t - \frac{\dot{\lambda}}{\omega_s}\sin\dot{\lambda}t) & 0 & 0 & \frac{\cos L}{\omega_s}\sin\omega_s t \\
\frac{\dot{\lambda}}{\omega_s}\sin L(\sin\omega_s t - \frac{\dot{\lambda}}{\omega_s}\sin\dot{\lambda}t) & \cos\omega_s t & \frac{\dot{\lambda}}{\omega_s}\cos L(\sin\omega_s t - \frac{\dot{\lambda}}{\omega_s}\sin\dot{\lambda}t) & -\frac{\dot{\lambda}^2}{\omega_s^2}(\cos\dot{\lambda}t - \cos\omega_s t) & 0 & -\frac{1}{\omega_s}\sin\omega_s t & 0 \\
\tan L(\cos\dot{\lambda}t - \cos\omega_s t) & -\sec L(\sin\dot{\lambda}t - \frac{\dot{\lambda}}{\omega_s}\sin^2 L\ \sin\omega_s t) & \cos\dot{\lambda}t & -\sec L(\sin\dot{\lambda}t - \frac{\dot{\lambda}}{\omega_s}\sin^2 L\ \sin\omega_s t) & 0 & 0 & -\frac{\sin L}{\omega_s}\sin\omega_s t \\
\sin L(\sin\dot{\lambda}t - \frac{\dot{\lambda}}{\omega_s}\sin\omega_s t) & \cos\dot{\lambda}t - \cos\omega_s t & \cos L(\sin\dot{\lambda}t - \frac{\dot{\lambda}}{\omega_s}\sin\omega_s t) & \cos\dot{\lambda}t & 0 & \frac{1}{\omega_s}\sin\omega_s t & 0 \\
\sec L(\cos\omega_s t - \cos^2 L - \sin^2 L\ \cos\dot{\lambda}t) & \tan L(\sin\dot{\lambda}t - \frac{\dot{\lambda}}{\omega_s}\sin\omega_s t) & \sin L(1 - \cos\dot{\lambda}t) & \tan L(\sin\dot{\lambda}t - \frac{\dot{\lambda}}{\omega_s}\sin\omega_s t) & 1 & 0 & \frac{1}{\omega_s}\sin\omega_s t \\
\dot{\lambda}\sin L(\cos\dot{\lambda}t - \cos\omega_s t) & \omega_s\ \sin\omega_s t & \dot{\lambda}\cos L(\cos\dot{\lambda}t - \cos\omega_s t) & -\dot{\lambda}(\sin\dot{\lambda}t - \frac{\dot{\lambda}}{\omega_s}\sin\omega_s t) & 0 & \cos\omega_s t & 0 \\
-\omega_s\sec L(\sin\omega_s t - \frac{\dot{\lambda}}{\omega_s}\sin^2 L\ \sin\dot{\lambda}t) & \dot{\lambda}\tan L(\cos\dot{\lambda}t - \cos\omega_s t) & \dot{\lambda}\sin L(\sin\dot{\lambda}t - \frac{\dot{\lambda}}{\omega_s}\sin\omega_s t) & \dot{\lambda}\tan L(\cos\dot{\lambda}t - \cos\omega_s t) & 0 & 0 & \cos\omega_s t
\end{bmatrix}$$

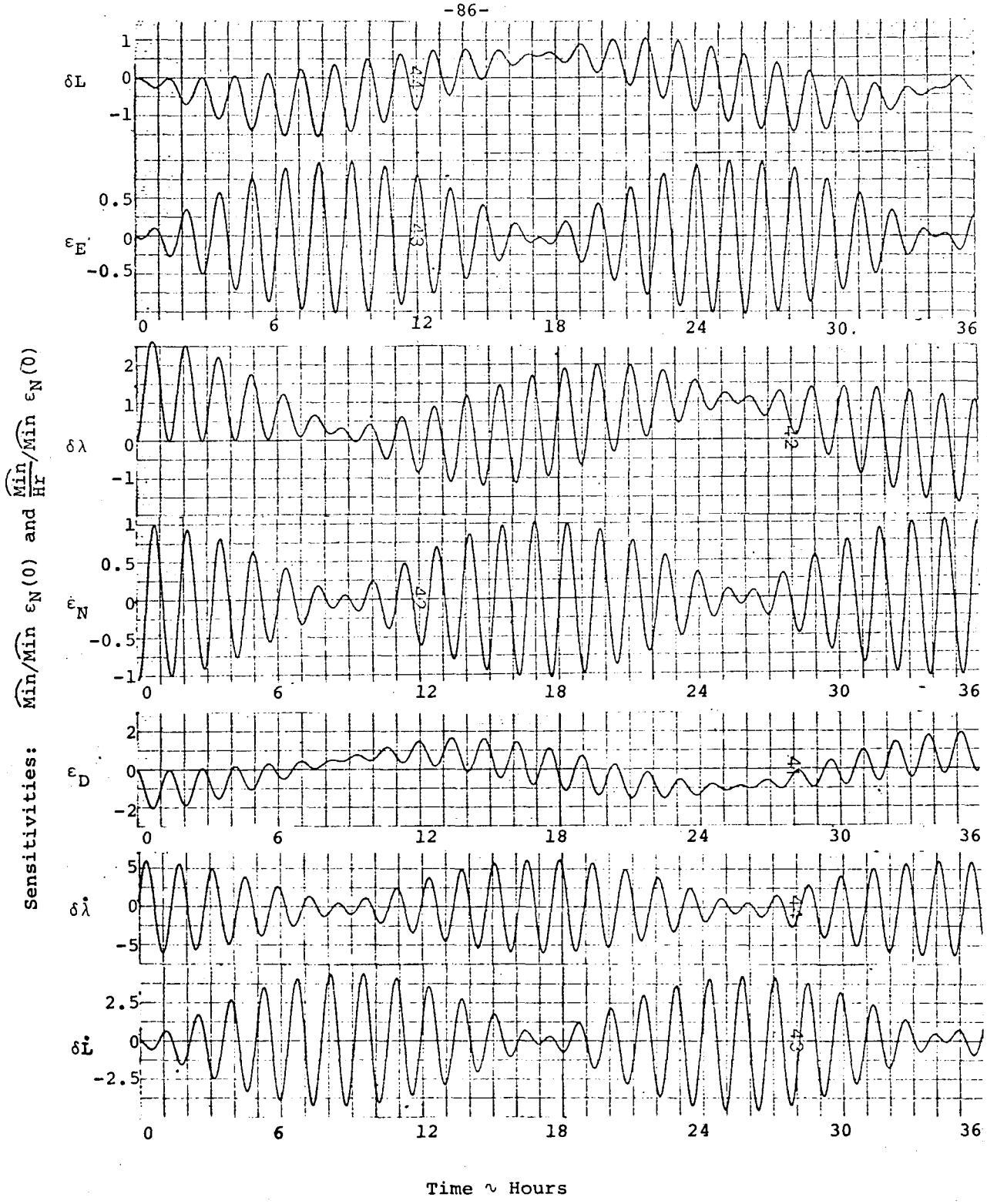


Figure 2.17 ∿ System Errors for Initial North Level Errors

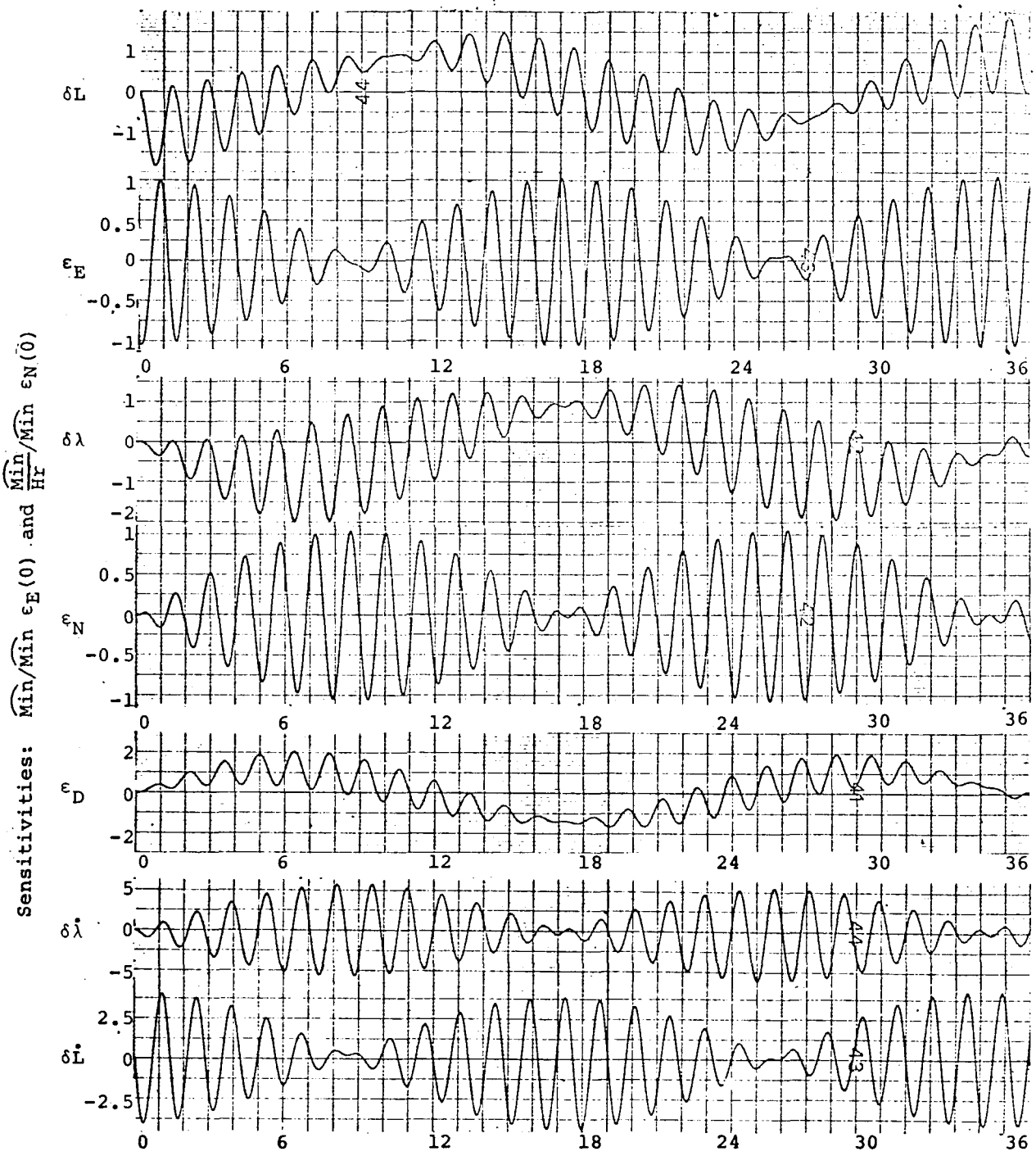


Figure 2.18 ∿ System Errors for Initial East Level Errors

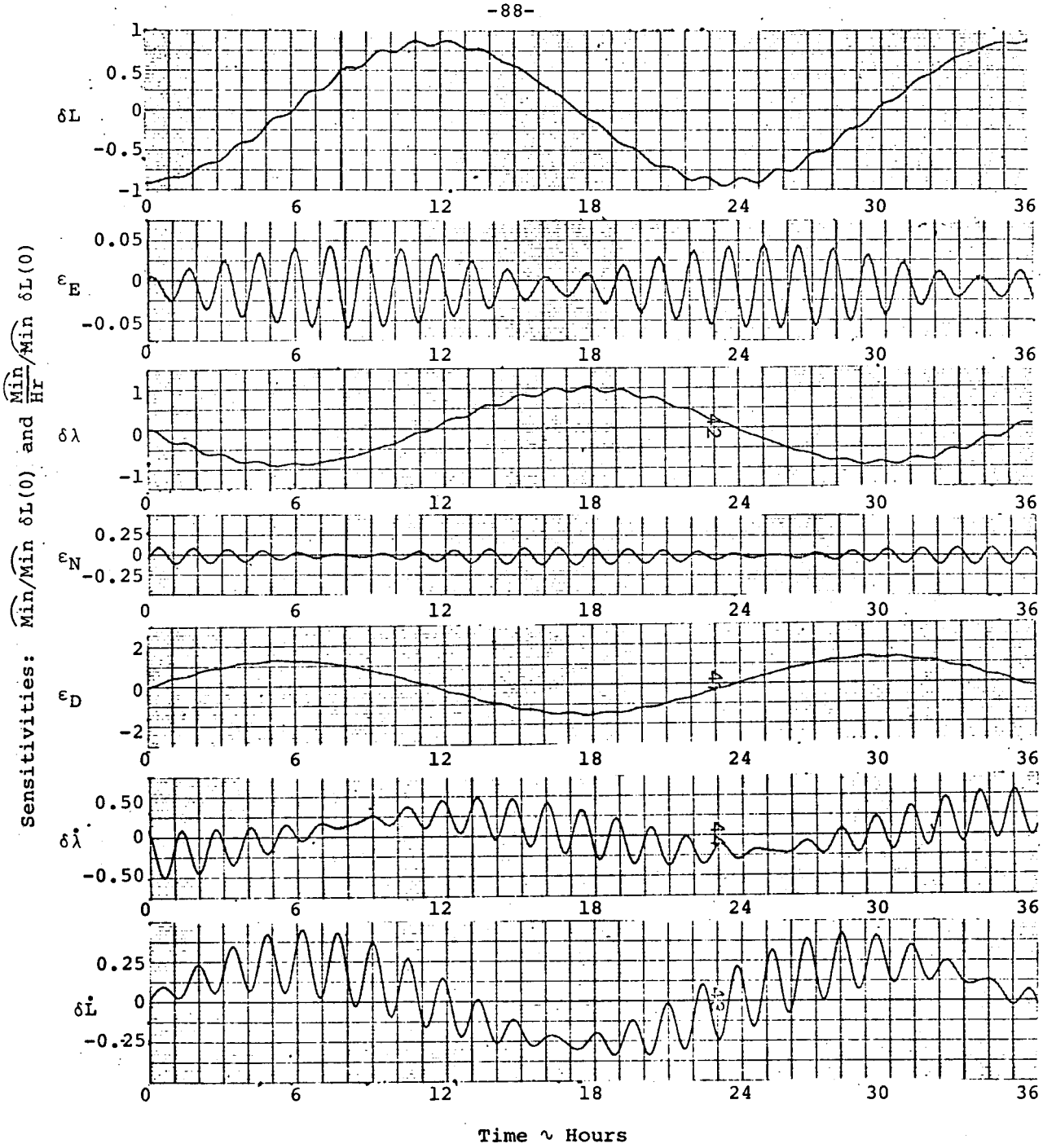


Figure 2.19 ∿ System Errors for Initial Latitude Errors

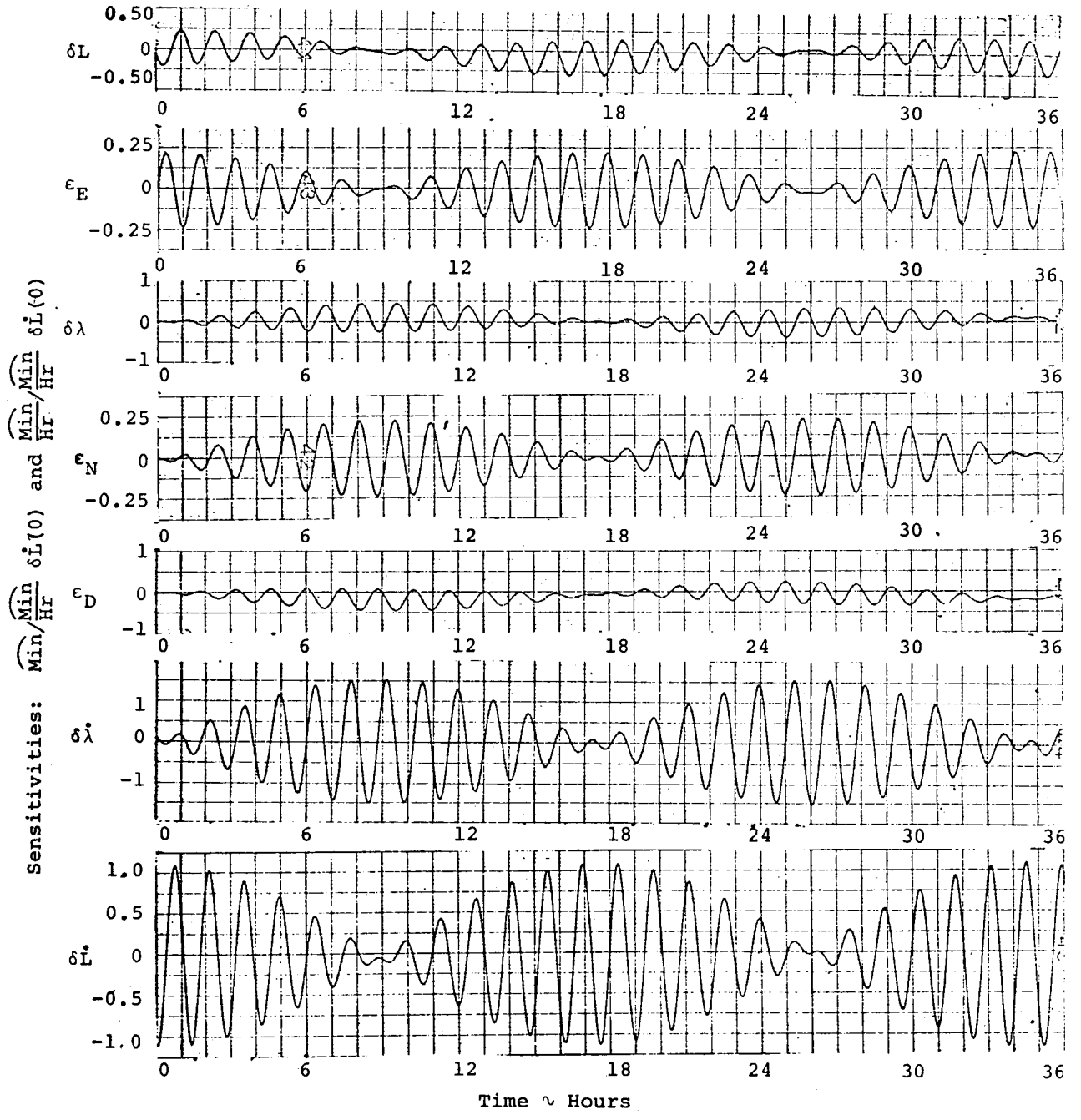


Figure 2.20 ∿ System Errors for Initial Latitude Rate Errors

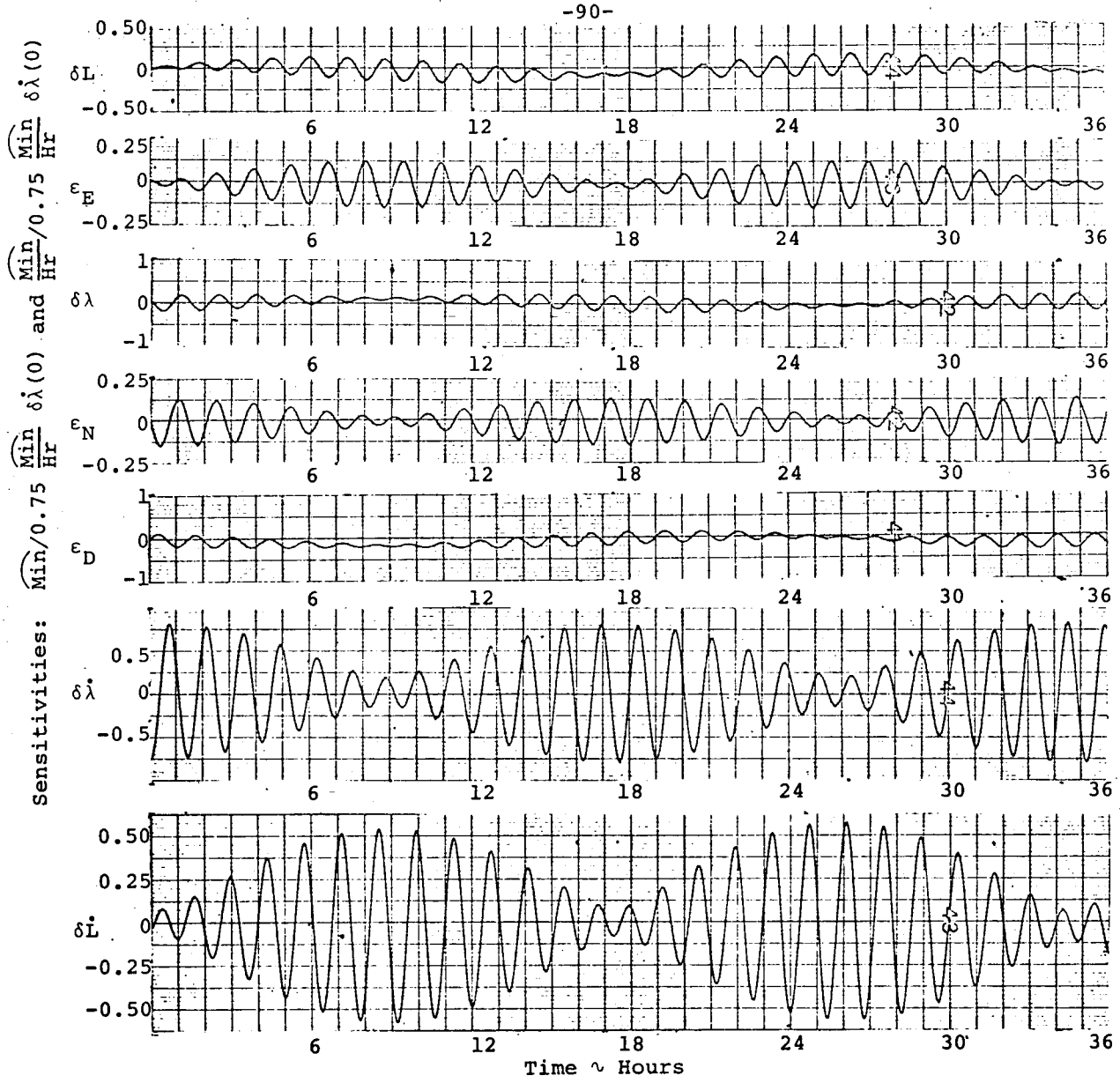


Figure 2.21 ∿ System Errors for Initial Longitude Rate Errors

REFERENCES

1. Britting, "Analysis of Space Stabilized Inertial Navigation Systems," MIT Experimental Astronomy Laboratory Report RE-35, Jan. 1968.

2. Markey and Hovorka, The Mechanics of Inertial Position and Heading Indication, Methuen, 1961.

3. Lipton, "Alignment of Inertial Systems on a Moving Base," MIT Sc.D. Thesis, Instrumentation Laboratory Report T-400.

4. Britting, "Strapdown Navigation Equations for Geographic and Tangent Coordinate Frames," MIT Measurement Systems Laboratory Report RE-56, June, 1969.

5. Wrigley, W., "Single Degree of Freedom Gyroscope," MIT IL Report R-375, July 1962.

6. Gianoukos and Palmer, "Gyro Test Laboratory Unbalance Equations," MIT IL Report GT-130, 1957.

7. Vahlberg, C., "Computer Compensation of Gyroscope Compliance Drift, MIT IL Report T-464, 1966.

8. Thompson and Unger, "Inertial Sensor Performance in a Strapped Down Environment," AIAA G. & C. Conference, 1966.

9. Weiner, "Theoretical Analysis of Gimballess Inertial Reference Equipment Using Delta Modulated Instruments," Sc.D. Thesis, MIT Department of Aeronautics and Astronautics, 1962.

10. Christianson, "Advanced Development of E.S.G. Strapdown Navigation Systems," Trans. IEEE, Vol. AES 2, No. 2, March 1966.

11. Britting and Palsson, "Self Alignment Techniques for Strapdown Inertial Navigation Systems with Aircraft Application," MIT EAL Report RE-33, Nov. 1967.

12. Farrel, J., "Performance of Strapdown Inertial Attitude Reference Systems," AIAA G. & C. Conference, August 1966.

13. "Advanced S.S.T. Guidance and Navigation System Requirements Study," T.R.W. Report Submitted to N.A.S.A. E.R.C., March 1967.

14. Gilmore, J., "A Nonorthogonal Gyro Configuration," MIT M.S. Thesis, Department of Aeronautics and Astronautics, Jan. 1967.